BOLT BERANEK AND NEWMAN INC

CONSULTING · DEVELOPMENT · RESEARCH

NASA CR-114756

RELATION BETWEEN NEAR FIELD AND FAR FIELD ACOUSTIC MEASUREMENTS

By David A. Bies and Terry D. Scharton

Prepared under Contract NAS2-6726

BBN Report 2600

29 March 1974

(NASA-CR-114756) RELATION BETWEEN NEAR FIELD AND FAR FIELD ACOUSTIC MEASUREMENTS (Bolt, Beranek, and Newman, Inc.) 74 ~~73~~ p HC $6.75 CSCL 20A

N74-23276

Unclas
G3/23 39271

Submitted to:

National Aeronautics and Space Administration
Ames Research Center
Moffett Field, California 94035

Prepared by:

Bolt Beranek and Newman Inc.
21120 Vanowen Street
Canoga Park, California 91303

NASA CR-114756

RELATION BETWEEN NEAR FIELD AND FAR FIELD ACOUSTIC MEASUREMENTS

By David A. Bies and Terry D. Scharton

Prepared under Contract NAS2-6726

BBN Report 2600

29 March 1974

Submitted to:

National Aeronautics and Space Administration
Ames Research Center
Moffett Field, California 94035

Prepared by:

Bolt Beranek and Newman Inc.
21120 Vanowen Street
Canoga Park, California 91303

TABLE OF CONTENTS

SUMMARY

Several approaches to the problem of determining the far field directivity of an acoustic source located in a reverberant environment, such as a wind tunnel, are investigated analytically and experimentally. The decrease of sound pressure level with distance is illustrated; and the spatial extent of the hydrodynamic and geometric near fields, the far field, and the reverberant field are described. A previously-proposed analytical technique for predicting the far field directivity of the acoustic source on the basis of near field data is investigated. Experiments are conducted with small acoustic sources and an analysis is performed to determine the variation with distance from the source of the directionality of the sound field. A novel experiment in which the sound pressure measured at various distances from an acoustic driver located in the test section of the NASA Ames 40 x 80 ft wind tunnel is crosscorrelated with the driver excitation voltage is conducted in order to further explore the relationship between the acoustic near field, far field, and reverberant field components. Coherency analysis of wind tunnel acoustic data is discussed. Two porous pipe microphones delivered under this contract are described in the Appendix.

INTRODUCTION

There is a great deal of interest in obtaining acoustic data during wind tunnel tests. Wind tunnel acoustic tests are attractive, because the often very important effects of forward speed on sound radiation are simulated. Several studies have been conducted to assess the feasibility of making acoustic measurements in the NASA Ames 40 x 80 ft wind tunnel.[1,2] Acoustic measurements for three different full-scale aircraft in this tunnel agreed well with inflight acoustic data.[1,3,4]

However since most wind tunnels are not designed as acoustic test facilities, it is often difficult to obtain accurate and complete acoustic data. In particular, the measurement of the directionality of the sound radiated far from a source is frustrated in a wind tunnel environment by noise associated with the drive machinery, wind, and reverberation. The purpose of this program is to investigate techniques for predicting the far field directivity from the near field acoustic measurements which can be conveniently obtained in a wind tunnel environment.

The definition of the acoustic near field and far field is illustrated in Fig. 1. The solid curve in Fig. 1 represents the decrease in sound pressure level as one moves away from an acoustic source located in an enclosed space. The sound pressure level at each point may be represented as the sum of the direct acoustic field, shown by the dotted curve in Fig. 1, and the reverberant field, shown by the dashed line in Fig. 1. The direct field is defined as the acoustic field that would exist if no reflections were present, that is if the source were located in free space or in an anechoic room. The reverberant field is composed of acoustic waves which have undergone one or more wall reflections after leaving the source. The hall radius is defined as the distance away from the source at which the direct field and reverberant fields are of equal strength; the total sound pressure level is therefore 3 dB above the contribution of each.

The direct acoustic field may be divided into two parts, the near field and the far field. In the far field, where the distance to the source is much larger than the acoustic wave length and the characteristic dimension of the source, the acoustic pressure decreases inversely with distance from the source, e.g., the sound pressure level falls off 6 dB for doubling of distance. If the directionality of the source is measured in the far field by plotting the sound pressure level versus angle at a fixed radius, the shape of this plot, the directivity, will be independent of the measurement radius.

The acoustic near field may be divided into two regions: the hydrodynamic near field which extends approximately 1/4 of an acoustic wave length λ from the source, and the geometric near field which extends several source dimensions from the source. Depending on frequency and the size of the source, either the hydrodynamic or geometric near field may extend further from the source. In Fig. 1 the geometric near field extends further than the hydrodynamic near field, which is applicable to consideration of medium and high frequency noise radiated from relatively large wind tunnel test items.

In the hydrodynamic near field, a large part of the pressure fluctuation is associated with the forces required to accelerate the fluid. In this region the fluid motion may be viewed largely as sloshing of an incompressible fluid. Therefore the pressures and fluid motion do not represent disturbances which propagate to the far field. Directionality measurements in the hydrodynamic near field will in general bear little correspondence to the far field directivity. The pressure falls off faster than 1/r in the hydrodynamic near field.

In the geometric near field the pressure does not fall off uniformly as one moves away from the source but fluctuates with distance as shown in Fig. 1. These fluctuations are caused by the constructive and destructive interference of sound waves arriving at the measurement point from different regions of the source. Directionality measurements in the geometric field will have different shapes at different distances but must of course become identical to the far field directivity patterns as the measurement radius increases.

To illustrate near field and far field acoustic directionality measurements, we conducted some experiments in an anechoic room with an acoustical source consisting of a hollow aluminum sphere 10 cm in diameter in which a 1.3 cm hole was drilled, Fig. 2. The acoustic driver consisted of a small speaker approximately 2.5 cm in diameter mounted inside the sphere directly behind the hole. The transmission loss of the hollow sphere, which was .64 cm thick, was greater than 30 dB at the excitation frequency, so that nearly all the sound emanated from the hole. The sound pressure levels measured in the near field at a radius of 6.1 cm from the center of the sphere and in the far field at a radius of 61 cm from the center of the sphere are shown as a function of angle in Fig. 3. The speaker was excited with 1/3 octave band noise centered at 5000 Hz, with a voltage of .5 volts rms.

Since the acoustic wave length at 5000 Hz is 34,400 cm/sec divided by 5000 Hz = 6.88 cm, we expect the hydrodynamic near field to extend approximately $\lambda/4$ = 1.72 cm from the hole. Thus the near field measurement on a traverse 1.1 cm from the surface of the sphere is in the hydrodynamic near field for approximately the first 30° of arc and in the geometric near field for the remaining angular sector. The near field directionality measurement shown in Fig. 3 indicates high acoustic levels directly in front of the hole, a rapid decrease in sound pressure level for the first 30° of arc, a more gradual reduction in level as one moves through the remaining 150° of arc, and some fluctuations in the acoustic level measured at the back side of the sphere. The measured SPL peaks on the back side of the sphere directly opposite the hole showing the effect of constructive interference of the waves generated by the source.

The acoustic directionality measured at a radius of 61 cm shows a much more uniform distribution of acoustic energy with angle and is probably a good approximation to the far field directivity of the source. The sound pressure levels measured directly in front of the hole have dropped approximately 20 dB as the radius is increased by a factor of 10 which happens to correspond exactly to the 1/r falloff of pressure with distance appropriate to the far field. However the sound pressure levels measured at the back side of the sphere directly opposite the hole increased 5 dB as the radius was increased by a factor of 10.

Now consider the measurement of acoustic directionality in the near and far field in a wind tunnel environment where one has to confront the problems of reverberation. Let us scale the results presented in Fig. 3 to a situation which might be of interest in the NASA Ames 40 x 80 ft wind tunnel. There a typical acoustic source might be of order 1 meter in radius or 20 times the size of the spherical source illustrated in Fig. 2. If the source were one meter in radius instead of 5 cm, the near field and far field directionality data presented in Fig. 3 would correspond to measurements 1.2 meters and 12 meters from the source respectively, with the source excited with third-octave band excitation centered at 250 Hz.

Figure 4 is a plan view of the NASA Ames 40 x 80 ft wind tunnel, and Fig. 5 shows the sound pressure levels measured at various stations in the tunnel with a dodecahedron sound source excited with 1/3-octave band noise centered at 250 Hz mounted in the center of the test section. Also shown in Fig. 5 is the free field calibration for the dodecahedron source which has a fairly omnidirectional radiation pattern.

The data in Fig. 5 indicate that the direct field governs the tunnel sound pressure levels within a distance of approximately 3 meters downstream of the omnidirectional source; the hall radius is approximately 4.6 meters. Since the acoustic wavelength at 250 Hz is 1.4 meters, the hydrodynamic near field would extend approximately .34 meters from the source at 250 Hz.

Measurements at higher frequencies in the 40 x 80 ft tunnel indicate that the hall radius does not vary significantly at frequencies below 4000 Hz. If a directional source is used instead of an omnidirectional source, the hall radius would be greater in a direction corresponding to the maximum radiation axis of the source, and smaller in the direction corresponding to minimum radiation directions.

The reverberant field data in Fig. 5 shows a general decrease in level as one moves upstream or downstream from the source. A large closed circuit wind tunnel, such as the Ames 40 x 80 ft wind tunnel, behaves like a reverberant room in the transverse directions but somewhat like a progressive wave tube in the axial direction. The falloff in acoustic energy with distance is less when the tunnel levels are corrected for the increase in tunnel cross section as shown by the solid dots in Fig. 5.

The foregoing considerations suggest that for typical acoustic sources of interest in the Ames 40 x 80 ft tunnel, acoustic measurements can conveniently be made at distances great enough to avoid hydrodynamic near field problems but not at great enough distances to avoid geometric near field effects on the measured directionality. In the remainder of this report we examine several techniques for determining the acoustic far field directivity using near field acoustic data which could be measured in a typical wind tunnel environment.

In the second section, an analytical technique for predicting the far field using near field acoustic data is investigated. In the third section, the errors involved in approximating the far field directivity with measurements of the directionality in the geometric near field are analyzed and near field and far field directionality data are compared. In the fourth section, a technique for crosscorrelating far field and near field acoustic signals to eliminate the effects of reverberation and tunnel noise is analyzed, and cross correlation data obtained in the Ames 40 x 80 ft wind tunnel with an electronic sound source is presented. The Appendix discusses the fabrication and calibration of two porous pipe microphones designed to discriminate against wind noise.

ANALYTICAL PREDICTION OF FAR FIELD USING NEAR FIELD DATA

A series expansion method[5,6] for predicting the far field from near field measurements was explored, using a small "lollipop" shaped acoustic source, the directivity of which exhibited multiple lobes. The total output in watts per volt input was determined from far field measurements of the source excited with 1/10 octave band and pure tone excitation at 5000 Hz in an anechoic facility. The mean square pressures were measured at fifteen positions on each of two radii in the near field of the source.

Following the analysis of Refs. 5 and 6, the pressure field of this axisymmetric source was represented by a modal expansion involving the spherical wave functions, i.e., Hankel functions in the radial direction and the Legendre polynomials in the zenithal direction. Using the representation of Ref. 6, modal expansions for the mean square pressure were developed. The modal expansion was terminated after 15 terms, and an attempt was made to determine the first five modal participation coefficients from the values of the mean square pressure measured at 15 points in the near field.

A computer program for accepting the data and inverting the resulting 15 x 15 matrices was developed and checked.

Computations were carried out for four sets of near field pressure data (each set involved measurements at 15 near field points). In each case nonsensical values of the modal participation coefficients were calculated. The reason for the failure of the technique is not known. It may be that the modal expansion employed converges very slowly, so that the truncation caused the problem. Alternately, inherent inaccuracies in the input near field data may have been responsible for failure of the technique. In any case, on the basis of this investigation, this analytical technique is not recommended for implementation in a wind tunnel environment.

Construction and Calibration of Acoustic Models

The instrumentation used to measure the near and far field pressures radiated from the model acoustic sources is shown in Fig. 6. The instrumentation for pure tone excitation included a sinewave generator, a power amplifier, and a voltmeter for determining the source input. Alternately for noise excitation, the instrumentation included a broadband noise generator, a tenth-octave band filter, an amplifier, and a voltmeter. The pressure measurement instrumentation included a quarter-inch B & K condenser microphone, a cathode follower type preamplifier, a sound level meter, an octave band filter, and a graphic level recorder configured for circular plots. The graphic level recorder was connected to a B & K turntable which rotated the acoustic models in synchronism with the circular plots.

Three acoustic models were fabricated and tested. First, the spherical source shown in Fig. 2 and described in the introduction was fabricated and tested. It was decided that the near and far field directionality patterns shown in Fig. 3 for the spherical source did not exhibit enough character to provide a valid test of the analytical far field prediction technique.

The second acoustic model was similar to the spherical model except that a second hole and speaker was positioned on the opposite side of the sphere from the first, and the two speakers were driven 180° out of phase to create dipole radiation. Although the radiation patterns from this source exhibited more character than that from the spherical source, it was determined that this source was not suitable for the analytical investigation since its radiation pattern was so similar to that of a classical dipole that the modal expansion would include only one term.

The acoustic model selected for investigation is shown in Fig. 7. This model which we designate the "lollipop" source consists of a speaker approximately 6 cm in diameter enclosed in a shallow aluminum cylinder 3.3 cm deep and 7 cm in diameter covered with a face plate 10.2 cm in diameter. The face plate contains a central hole .75 cm in diameter and 33 small holes .5 cm in diameter equally spaced on a 5 cm diameter circle. The radiation pattern of this model is symmetrical about the axis of the cylinder.

The far field sound radiated by this model was measured on a circle of radius 75 cm located in the horizontal plane intersecting the cylinder axis. The measured far field pressure levels are shown in Figs. 8 and 9 for pure tone and tenth-octave excitation centered at 5000 Hz. The sound power P radiated by the lollipop source was determined from the expression

$$P = \frac{2\pi R^2}{\rho c} \int_0^\pi p^2(\theta) \sin\theta \, d\theta \qquad (1)$$

where ρc is the acoustic impedance, R is the far field radius, and $p^2(\theta)$ is the mean square pressure at angle θ. Applying Eq. 1 to the far field data presented in Figs. 8 and 9 and noting that the acoustic model was driven with .3 rms volts, we calculate the sensitivity as PWL=58 dB re 10^{-12} watts/ volts^2.

Near Field Acoustic Measurements

The near field acoustic pressure measured as a function of angle at radii of 6.66 cm and 7.92 cm from the center of the lollipop source are shown in Fig. 8 for pure tone random excitation and in Fig. 9 for tenth-octave band excitation. Table I shows the numerical values of the mean square pressure read from the raw data presented in Figs. 8 and 9. The data were read at 15 angular positions for each of the two radii. The two measurement radii and the 15 angular positions were chosen to facilitate the use of tabulated values of the Hankel functions and the Legendre polynomials.

The radial positions are normalized by the acoustic wavelength:

$$\xi \equiv \frac{2\pi R}{\lambda}$$

The acoustic wavelength for pure tone excitation at 5000 Hz was measured as 6.64 cm which compares with the theoretical value of 34,400 cm/sec divided by 5000 Hz = 6.88. Using the measured value of the acoustic wavelength the value of ξ corresponding to the 6.66 cm radius is $\xi = 6.3$ and the value corresponding to the 7.92 cm radius is $\xi = 7.5$.

The data presented in Table I were obtained from the raw directionality measurements in the following manner. First the dB levels associated with the 15 angular measurement positions were read from the raw data independently by two workers.

Table I - Numerical Values of Near Field Data

Angular Msmt Locations		1/10 Octave Excitation				Pure Tone Excitation			
		$\xi = 6.3$		$\xi = 7.5$		$\xi = 6.3$		$\xi = 7.5$	
No.	Degrees	dB	Linear	dB	Linear	dB	Linear	dB	Linear
1	0	0	1.00	-0.5	0.87	0	1.00	-2.0	0.62
2	25.84	-0.25	0.96	0.25	1.05	+0.5	1.10	-1.0	0.77
3	51.68	-0.25	0.96	0.25	1.05	+0.1	1.02	-1.0	0.77
4	77.29	-12.0	0.062	0.75	1.15	-11.7	0.066	-10.5	0.086
5	102.71	-17.0	0.020	-8.75	0.13	-16.5	0.022	-17.7	0.017
6	128.32	-18.0	0.016	-16.5	0.022	-16.5	0.022	-17.3	0.018
7	154.16	-18.5	0.014	-16.25	0.023	-20.5	0.0086	-20.2	0.0093
8	180	-13.0	0.050	-17.25	0.018	-13	0.050	-13	0.050
9	14.07	-0.25	0.96	-14.5	0.035	+0.2	1.04	-1.8	0.64
10	38.74	0.75	1.15	-0.25	0.96	+0.9	1.18	-0.3	0.90
11	64.53	-4.25	0.37	1.50	1.35	-4.0	0.38	-4.2	0.37
12	90.0	-18.0	0.016	-3.25	0.47	-20.5	0.0088	-17.8	0.016
13	115.47	-16.0	0.025	-15.75	0.026	-14.8	0.033	-15.9	0.026
14	141.26	-22.75	0.0053	-20.5	0.0089	-23.5	0.0044	-24.3	0.0036
15	165.93	-14.25	0.037	-12.75	0.053	-15.2	0.030	-14.9	0.032

The two dB levels were averaged and referenced to a zero dB level at $\xi = 6.3$ and $\theta = 0$. The linear values of the mean square pressure were then computed from the dB levels to two significant figures.

Analysis

For sinusoidal excitation of an axially symmetric source, the pressure as a function of radius, angle measured from the axis of symmetry, and time can be expressed as

$$p(R,\theta,t) = \sum_{n=0}^{\infty} C_n h_n(\xi) P_n(\eta) e^{-i\omega t} \qquad (3)$$

where C_n is a modal participation coefficient of the *nth* mode, h_n is the spherical Hankel function of order n, and P_n is the Legendre function of order η. The argument of the Hankel function is the normalized radius ξ defined in Eq. 2 and the argument of the Legendre function η is defined as the cosine of the angle θ. The modal coefficients and the Hankel functions are both complex numbers.

The mean square pressure at the point (R, θ) is given by

$$\overline{p^2(R,\theta)} = \frac{1}{2} [pp^*]$$

$$= \frac{1}{2} \sum_{n=0}^{\infty} \sum_{m=0}^{\infty} C_n C_m^* h_n(R) h_m^*(R) P_n(\theta) P_m^*(\theta) \ . \qquad (4)$$

When the modal coefficients and Hankel function are expressed in terms of their real and imaginary parts

$$\begin{aligned} C_n &\equiv a_n + ib_n \\ &, \\ h_n &\equiv j_n + iy_n \end{aligned} \qquad (5)$$

the mean square pressure can be written as

$$\overline{p^2(R,\theta)} =$$

$$\frac{1}{2} \sum_n \sum_m [(a_n a_m + b_n b_m)(j_n j_m + y_n y_m) - (a_m b_n - a_n b_m)(j_m y_n - j_n y_m)] P_n P_m \, ; \qquad (6)$$

which with the definitions

$$\begin{aligned} A_{mn} &= A_{nm} = a_m a_n + b_n b_m \\ B_{mn} &= -B_{nm} = a_m b_n - a_n b_m \\ H_{mn} &= H_{nm} = j_n j_m + y_n y_m \\ K_{mn} &= -K_{nm} = j_m y_n - j_n y_m \end{aligned} \qquad (7)$$

can be expressed as

$$\overline{p^2(R,\theta)} = \frac{1}{2} \sum_{m=0}^{\infty} \sum_{n=0}^{\infty} [A_{mn} H_{mn} - B_{mn} K_{mn}] P_n P_m \, . \qquad (8)$$

The Hankel functions and Legendre polynomials can be expressed as power series of the form

$$\begin{aligned} h_r(\xi) &= f\left[\left(\frac{1}{\xi}\right)^{r+2}, \left(\frac{1}{\xi}\right)^{r+1}, \dots \left(\frac{1}{\xi}\right)\right] \\ P_s(\eta) &= g\left[\eta^s, \eta^{s-1}, \dots \eta^o\right] \end{aligned} \tag{9}$$

Therefore truncation of the double series given by Eq. (8) at $n + m = \ell$ retains terms of order $(1/\xi)^{\ell+2}$ and η^{ℓ}. Choosing $\ell = 4$ and taking advantage of the symmetry relations expressed by Eq. (7) indicates that the double sum in Eq. (8) will have 15 terms with 15 coefficients denoted by A_1 through A_{15} below.

$$\begin{array}{lll} A_1 = A_{00} & A_6 = A_{11} & A_{11} = A_{40} \\ A_2 = A_{10} & A_7 = A_{30} & A_{12} = -B_{40} \\ A_3 = -B_{10} & A_8 = -B_{30} & A_{13} = A_{31} \\ A_4 = A_{20} & A_9 = A_{21} & A_{14} = -B_{31} \\ A_5 = -B_{20} & A_{10} = -B_{21} & A_{15} = A_{22} \end{array} \tag{10}$$

Using the coefficients defined in Eq. (10) the final expression for the mean square pressure at (R,θ) is

$$\begin{aligned} \overline{p^2(R,\theta)} \simeq {} & A\ (j_0^2+y_0^2)P_0^2/2+A_2(j_1j_0+y_1y_0)P_1P_0+A_3(j_1y_0-j_0y_0)P_1P_0 \\ & + A_4(j_2j_0+y_2y_0)P_2P_0+A_5(j_2y_0-j_0y_2)P_2P_0+A_6(j_1^2+y_1^2)P_1^2/2 \\ & + A_7(j_3j_0+y_3y_0)P_3P_0+A_8(j_3y_0-j_0y_3)P_3P_0+A_9(j_2j_1+y_2y_1)P_2P_1 \\ & + A_{10}(j_2g_1-j_1y_2)P_2P_1+A_{11}(j_4j_0+y_4y_0)P_4P_0+A_{12}(j_4y_0-j_0y_4)P_4P_0 \\ & + A_{13}(j_3j_1+y_3y_1)P_3P_1+A_{14}(j_3y_1-j_1y_3)P_3P_1+A_{15}(j_2^2+y_2^2)P_2^2/2 . \end{aligned} \tag{11}$$

The spherical Bessel functions j and spherical Neumann functions y are evaluated at the radius R and the Legendre functions P are evaluated at the angle θ. The approach is to apply Eq. (11) at 15 points in the near field of the lollipop source and to use the measured mean square pressures at the 15 near field points to evaluate the 15 values of the coefficient A. The first five modal coefficients C_0, C_1, C_2, C_3, and C_4 would then be determined through the relations given in Eqs.(10), (7), and (5).

In order to apply this approach to the near field data presented in Figs. 8 and 9 for a pure tone and tenth-octave random excitation centered at 5000 Hz, we use the values of the Legendre function for the 15 measurement angles tabulated in Table II, the values of the spherical Bessel and Neumann functions tabulated in Table III for the measurements at a radius of 6.66 cm or $\xi = 6.3$ and for the measurements at a radius of 7.92 cm corresponding to $\xi = 7.5$.

A matrix for the Hankel and Legendre function coefficients in Eq. (11) were prepared for each of the following two column vectors of mean square near field pressure measurements. For Matrix 1: Rows 1 through 8 for the excitation vector corresponded to near field measurements at $\xi = 6.3$ at angular locations 1 through 8 and Rows 9 through 15 corresponded to measurements at $\xi = 7.5$ at angular locations 9 through 15. For Matrix 2: Rows 1 through 8 of the excitation vector corresponded to

TABLE II LEGENDRE FUNCTION VALVES

Measurement Point	Degrees	$P_1(\eta)$	$P_2(\eta)$	$P_3(\eta)$	$P_4(\eta)$
1	0	1.000	1.000	1.000	1.000
9	14.07	0.97	0.91135	0.82668	0.71978
2	25.84	0.90	0.71500	0.47250	0.20794
10	38.74	0.78	0.41260	0.01638	-0.28709
3	51.68	0.62	0.07660	-0.33418	-0.42004
11	64.53	0.43	-0.22265	-0.44623	-0.16880
4	77.29	0.22	-0.42740	-0.30338	0.20375
12	90.00	0.00	-0.50000	0.0000	0.37500
5	102.71	-0.22	-0.42740	0.30338	0.20375
13	115.47	-0.43	-0.22265	0.44623	-0.16880
6	128.32	-0.62	0.07660	0.33418	-0.42004
14	141.26	-0.78	0.41260	-0.01638	-0.28709
7	154.16	-0.90	0.71500	-0.47250	0.20794
15	165.93	-0.97	0.91135	-0.82668	0.71978
8	180	-1.000	1.000	-1.000	1.000

TABLE III. SPHERICAL BESSEL AND NEUMANN FUNCTION VALUES

ξ	m	j_m	y_m
6.3	0	.0026689	-.15871
6.3	1	-.15828	-.027861
6.3	2	-.078042	.14544
6.3	3	.096346	.14329
6.3	4	.18509	.013770
7.5	0	.12507	0.046218
7.5	1	.029542	-.13123
7.5	2	-.13688	-.0062736
7.5	3	-.061713	.12705
7.5	4	.079285	.12485

measurements at $\xi = 7.5$ at locations 1 through 8, and Rows 9 through 15 of the excitation vector corresponded to measurements at $\xi = 6.3$ at locations 9 through 15. Excitation vectors corresponding to these two matrices were constructed from the lollipop near field data tabulated in Table I for both pure tone and 1/10-octave band excitation centered at 5000 Hz -- thus four excitation vectors were constructed in all. The coefficients of Eq. (10) obtained by inverting the matrices formed from Eq. (11) for these four sets of data are shown in Table IV.

The results presented in Table IV are nonsensical because as Eq. (7) indicates the coefficients A_{00}, A_{11}, and A_{22}, must by definition be positive, and this is not the case for any of the four sets of results presented in Table IV. Thus it was not possible in any of the four test cases to solve Eq. (7) for the desired modal coefficients C_n of Eq. (5).

It is difficult to pinpoint with assurety the reason for the failure of this approach. The matrix inversion computer program was checked using a test matrix and it appeared to be working properly and the tabulated Hankel and Legendre functions seem correct.

A possible problem is associated with inaccuracies of the near field pressure data. A previous analytical investigation[5/] showed that rounding off the input near field data to two

Table IV - Modal Coefficient Results

Coefficient	Pure Tone		1/10 Octave Band	
	Matrix 1	Matrix 2	Matrix 1	Matrix 2
$A_{00}=$	$-0.109288x10^{8}$	$0.273265x10^{16}$	$0.338x10^{7}$	$0.214x10^{17}$
A_{10}	$0.512965x10^{6}$	$0.117591x10^{6}$	$-0.180x10^{6}$	$-0.279x10^{6}$
$-B_{10}$	$0.235705x10^{6}$	$0.280940x10^{5}$	$-0.159x10^{6}$	$-0.189x10^{5}$
A_{20}	$0.227734.10^{8}$	$-0.69569x10^{16}$	$-0.700x10^{7}$	$-0.545x10^{17}$
$-B_{20}$	$0.218717x10^{8}$	$-0.145330x10^{17}$	$-0.666x10^{7}$	$-0.134x10^{18}$
A_{11}	$0.465757x10^{8}$	$-0.114824x10^{17}$	$-0.144x10^{8}$	$-0.900x10^{17}$
A_{30}	$0.757115x10^{5}$	$-0.681467x10^{4}$	$-0.981x10^{5}$	$0.005x10^{5}$
$-B_{30}$	$-0.263427x10^{6}$	$-0.325323x10^{5}$	$0.175x10^{6}$	$0.255x10^{5}$
A_{21}	$-0.586749x10^{6}$	$-0.134297x10^{6}$	$0.206x10^{6}$	$0.317x10^{6}$
$-B_{21}$	$-0.579030x10^{6}$	$-0.678400x10^{5}$	$0.395x10^{6}$	$0.410x10^{5}$
A_{40}	$-0.383467x10^{3}$	$-0.121992x10^{16}$	$0.173x10^{3}$	$-0.960x10^{16}$
$-B_{40}$	$-0.163380x10^{8}$	$0.103583x10^{17}$	$0.494x10^{7}$	$0.812x10^{17}$
A_{31}	$-0.232345x10^{8}$	$0.842204x10^{16}$	$0.708x10^{7}$	$0.660x10^{17}$
$-B_{31}$	$-0.338396x10^{8}$	$0.221148x10^{17}$	$0.103x10^{8}$	$0.173x10^{18}$
A_{22}	$-0.230632x10^{8}$	$0.550619x10^{16}$	$0.713x10^{7}$	$0.432x10^{17}$

significant figures and introducing 1% errors in the definition of the near field measurement locations led to significant errors in the prediction of the far field radiation. Certainly in our experiments as in a wind tunnel, a two significant figure accuracy in the input data and 1% accuracy in the definition of measurement locations would be difficult to realize.

A second possible problem in our investigation concerns the limited number of measurement points and consequently the limited number of terms retained in the modal expansion of Eq. (8).

A limited amount of attention was also directed to investigating the alternative representation of Ref. 5 which involves the use of pressure cross-power data measured for various pairs of points in the near field. The cross-power method offers the potential advantage that fewer microphone positions are required to generate a given amount of data than are required with the mean-square pressure technique. However the data analysis equipment necessary to calculate cross-power is obviously more complex than that required to calculate mean-square pressures. Our test of the cross-power method was very similar to that described previously for the mean-square method. Negative results were again obtained.

DIRECT COMPARISON OF NEAR FIELD AND FAR FIELD DIRECTIVITIES

The difficulties encountered in the analytical technique explored in the last section lead us to explore other techniques for determining the far field radiation pattern from near field measurements in a wind tunnel environment. In a wind tunnel the near field measurement errors typically encountered are those associated with the geometric field rather than those encountered with the hydrodynamic field, see Fig. 1. Therefore we have conducted some experiments and developed an analysis to illustrate the types of errors associated with geometric near field directivity measurements.

The results of these model experiments and the analysis indicate that the directionality measurements which could be obtained approximately 1 hall radius from the source in a tunnel such as the Ames 40 x 80 ft wind tunnel represent reasonable approximations to the far field directivity. This is true particularly for the purposes of finding the major lobes in the radiation patterns. The directivity notches for aircraft signatures are of less interest, because in almost every case, the major radiation peak determines the perceived noise levels on the ground.

Analysis

Herein we analyze the errors involved in deducing the far field sound directivities from acoustic data measured a few source diameters from the sound source. We assume that the measurement point is many acoustic wavelengths away from the source so that the hydrodynamic near field errors are not a problem.

A typical sound source of interest might be a helicopter rotor (of radius a). We shall suppose that measurements are averaged over a sufficient time (more than a fraction of the period of the rotor's rotation) so that the sound source appears to be a circular disk.

In the problem described the sound actually emanates from patches or regions in the plane of the rotor where the characteristic length (the correlation length) of the sound sources is small compared with the radius of the rotor. Accordingly for the purposes of making reasonable estimates of the errors involved in the measurement we shall suppose that the sources are distributed uniformly over the area of the disk and are of such a nature that we can suppose that the sources at neighboring points are phase incoherent. Errors made due to coherence will be slight under the described conditions.

We shall test errors in the deduction of the far field behavior: for a constant amplitude *simple* source distribution in the disk; for a constant *dipole* source, with the axis of the dipole perpendicular to the disk; and for a constant longitudinal *quardupole* source distribution again with the axis perpendicular to the disk. We shall see that the errors made in the deduction of the far field are least for the simple sources and greatest for the quadrupoles.

To begin let $I_0 dS$ be the sound field intensity observed on the source axis at unit distance from the source for source element dS. Consider an observation point P located a distance r and at an angle θ' from the rotor axis (Fig. 10). Of course the angle to the observation makes no difference for the simple source distribution. The sound field intensity at the point P is given by

$$I_{\substack{SS\\ D.\\ Q.}}(P) = \iint\limits_{\substack{\text{Disk of}\\ \text{radius } a}} dS \, \frac{I_0}{(r')^2} \begin{Bmatrix} 1 \\ \cos^2\theta' \\ \cos^4\theta' \end{Bmatrix} \tag{12}$$

Quantities in the bracket within the integral are associated respectively with the intensity due to a simple source, a dipole, and a quadrupole distribution. In Eq.(12) r' is the distance from the source region to the observation point P, and θ' is the observation angle with the normal.

As seen in Fig. 10, the point P has been placed in the y-z plane, which can be done without loss of generality for the axially-symmetric sound source considered here. The angle θ is the polar angle for the observation point; $\underline{r}$ is the distance of the observation point from the center of the source distribution, the rotor in this example. The vector $\underline{\rho}$ is the displacement of the element dS from the origin; $\hat{k}$ is the unit vector in the z direction and r' is the vector distance from dS to P.

Our problem is now to evaluate the integrals in Eq. (12) in terms of the field coordinates r and θ. To do so, note

$$r'\cos\theta' = \underline{r}'\cdot\hat{k} = r\cos\theta \tag{13}$$

where we use the relation

$$\underline{r}' = -\underline{\rho} + \underline{r}. \tag{14}$$

Further note that

$$\underline{\rho}\cdot\underline{r} = \rho r\sin\theta\cos\alpha \tag{15}$$

Substitute these quantities in Eq. (12) to find

$$\begin{matrix} I_{SS} \\ D \\ Q \end{matrix} = \frac{I_0 \pi a^2}{r^2} \begin{Bmatrix} \mathcal{J}_1 \\ \cos^2\theta\,\mathcal{J}_2 \\ \cos^4\theta\,\mathcal{J}_3 \end{Bmatrix} \tag{16}$$

with

$$\mathcal{J}_n \equiv \frac{r^2}{\pi a^2}\int_0^{2\pi} d\alpha \int_0^{a/r} \xi d\xi\ [1 - 2\xi\sin\theta\cos\alpha + \xi^2]^{-n} \tag{17}$$

where n takes on the values 1, 2, 3 and $\xi \equiv \rho/r$.

The decibel error in the far field sound deduced from the near field measurement is given by

$$dB_{E,n} = 10 \log \mathcal{I}_n \tag{18}$$

where the simple source, dipole source, and quadrupole source are found using n = 1, 2, 3, respectively. A positive error indicates that the near field measurement is higher than it would have been if the entire source had the same power but was concentrated at the origin.

We could of course integrate Eq. (17) numerically; however, and more simply, we can take a power series expansion since we are primarily interested in field points such that $\frac{a}{r}$ is a number less than 1. We do this finding the power series expansion

$$\begin{aligned}
[1-2\xi \sin\theta \cos\alpha+\xi^2]^{-n} &= 1+2\xi n \sin\theta \cos\alpha + \\
&+\xi^2[-n+2n(n+1) \sin^2\theta \cos^2\alpha] + \\
&+\xi^3[-2n(n+1) \sin\theta \cos\alpha + \tfrac{4}{3} n(n+1)(n+2) \sin^3\theta \cos^3\alpha] + \\
&+\xi^4[\tfrac{n(n+1)}{2} - \tfrac{2}{3} n(n+1)(n+2) \sin^2\theta \cos^2\alpha \\
&\qquad + \tfrac{2}{3} n(n+1)(n+2)(n+3) \sin^4\theta \cos^4\alpha] + O(\xi^5).
\end{aligned} \tag{19}$$

Substitute (19) in (17) and integrate to find

$$\begin{aligned}
\mathcal{I}_n = 1 - \frac{n}{2} [1-(n+1) \sin^2\theta] \left(\frac{a}{r}\right)^2 + \frac{n(n+1)}{6} [1 - \frac{2(n+2)}{3} \sin^2\theta \\
+ \frac{1}{2} (n+2)(n+3) \sin^4\theta] \left(\frac{a}{r}\right)^4 + O\left(\frac{a}{r}\right)^6 .
\end{aligned} \tag{20}$$

Use (20) in (18) to obtain

$$dB_{E,n} \simeq 10 \log_{10} \left\{ 1- \frac{n}{2} [1-(n+1) \sin^2\theta] \left(\frac{a}{r}\right)^2 \right\} \tag{21}$$

valid when

$$\frac{n(n+1)}{6} [1 - \frac{2}{3} (n+2) \sin^2\theta + \frac{1}{2} (n+2)(n+3) \sin^4\theta] \left(\frac{a}{r}\right)^4$$

is smaller than one.

It is recalled that in Eq. (21) $n = 1$ gives the error for a simple source distribution, $n = 2$ gives the error for a dipole source distribution, and $n = 3$ gives the error for a quadrupole source. As an example we see from (21) setting $n = 1$, (for a simple source distribution) that if our field point is of one diameter distance from the center of the rotor disk and on the axis of the disk ($\theta = 0$), the error is a little more than 1 dB: i.e., negligible in the usual practical situation. The error has the same magnitude but opposite sign for $\theta = 90°$ (P in the x-y plane). We see that for a field point located 1-1/2 diameters from the center of the disk, on the axis of the disk, the error for a quadrupole source ($n = 3$) is about 1-1/2 dB, again negligible in practice.

Experiments

We conducted a simple experiment to illustrate the size of the errors involved in using geometric near field directionality plots to approximate the far field directivity. The experiments were conducted in the anechoic room using an inexpensive unbaffled acoustic speaker of radius $a = 15$ cm. The speaker was excited with 1/3-octave band of noise centered at 4000 Hz and the directionality of the acoustic field was measured at distances 15, 30, 60, and 240 cm from the speaker center corresponding to r/a = 1, 2, 4, and 16. The directionality plots measured at these distances with a B & K 1/2-inch microphone are shown in Fig. 11, and those measured with a special porous pipe microphone described in the appendix are shown in Fig. 12. The data presented in Figs. 11 and 12 have been normalized so that at each radius the peak in the radiation lobe at $\theta=0$ has the same level.

Let us scale these experiments by a factor of 20 in order to apply the results to a situation of typical interest in the Ames 40 x 80 ft wind tunnel. With that purpose we consider a source with a radius a' = 3 meters with a predominant acoustic radiation frequency of 200 Hz. The data presented in Figs. 11 and 12 for measurements at r/a = 1, 2, 4, and 16 represent measurements at distances 3, 6, 12, and 48 meters from the center of the source located in the tunnel respectively.

Consider a source located directly in the center of the 40 x 80 ft. tunnel test section. If measurements are conducted in the horizontal plane, measurements could be conducted 12 meters from the source without interfering with the tunnel walls, but if measurements are conducted in the vertical plane the radius must be restricted to 6 meters from the center of the source. However the data presented in Fig. 5 indicates that for an omnidirectional source located in the center of the Ames 40 x 80 ft tunnel, the direct field extends approximately only 3 meters downstream of the source for the 250 Hz excitation case. Thus without the use of special directional microphones such as an endfired or broadside fired array, or long shotgun microphone, directionality measurements would be restricted to a radius 3 meters from the center of the source or at r/a corresponding to 1 in Figs. 11 and 12. The directionality plot corresponding to r/a = 1 in Fig. 11 is reasonably similar to that measured in the far field at r/a = 16. The near field and far field directionality plots measured with a directional microphone and shown in Fig. 12 are in even closer agreement.

The data shown in Figs. 11 and 12 do however show greater errors involved in the near field measurements than predicted in the preceding analysis which assumed that the radiating disk consisted of a number of small independent source regions. We attempted to simulate this situation in our experiments by using a large inexpensive hi-fi speaker whose cone breaks up into many incoherent patches when excited with high frequency sound. The difference between the measured and predicted near field errors probably reflects the sensitivity of the near field errors to the size and number of the independent radiation regions contained in a distributed source.

CROSSCORRELATION OF NEAR FIELD AND FAR FIELD ACOUSTIC MEASUREMENTS IN A WIND TUNNEL ENVIRONMENT

Some preliminary experiments were conducted in the NASA Ames 40 by 80 foot tunnel to explore the possibility of using cross-correlation techniques to measure the direct acoustic field in the presence of tunnel noise, wind noise, and reverberation. We first present two analyses. The first demonstrates that cross-correlation between the source and receiver signal is a useful tool for discriminating against wind noise, tunnel noise, and reverberation. The second demonstrates that coherency analysis is a useful tool for source identification in the presence of reverberation. These analyses indicate that the combination of correlation and coherency analyses provides a very powerful technique for determining the directivity of the radiation from individual aerodynamic sources associated with an aircraft in a wind tunnel test configuration.

Crosscorrelation Analysis

Consider sound radiation to an observation point P located in the far field of a source i which is one of many independent sources distributed throughout a given source region, as shown in Figure 13. It is assumed that the observation point P is in the far field i.e. that the distance R is large compared to both the acoustic wave length and the characteristic dimension of the source region. For simplicity we assume that the i sources are monopoles in this analysis, but the results apply for other types of sources as well.

The pressure at the observation point P due to the ith source is given by

$$p_i(\bar{R}|\vec{r}_i,t) = S_i(t - \frac{\xi_i}{c})\ \gamma_i(\xi_i,\ t) \tag{23}$$

where S_i is the volume velocity of the *ith* source and γ_i is given by

$$\gamma_i(\xi_i,\ t) = -i\omega\rho\ \frac{e^{i\omega(\xi_i/c-t)}}{4\pi\xi_i} \tag{24}$$

where ω is the radian frequency, ρ is the acoustic density, and c is the speed of sound. The total pressure at the observation point is equal to the sum of the contributions from the individual sources

$$p(\bar{R},t) = \sum_{i=1}^{N} S_i(t - \frac{\xi_i}{c})\ \gamma_i(\xi_i,t) \tag{25}$$

Since the sources are uncorrelated we have

$$<S_i\ S_j> = S^2\ \delta_{ij}\ , \tag{26}$$

where the brackets indicate ensemble averaging and δ_{ij} is a Kronecker delta function equal to unity if i=j and equal to 0 if i≠j. Multiplying both sides of Eq. (25) by the pressure p(R) we have for the mean square pressure at the observation point

$$\overline{p}^2(R,t) = \sum_{i=1}^{N} \langle S_i \ p\rangle \gamma_i = \sum_{N=i}^{N} p_i^2 \tag{27}$$

Thus because of the assumed independence of the sources the total pressure at the observation point is simply the sum of the mean square pressure resulting from each source. Combining Eqs. (23) and (27) the contribution to the mean square pressure at the observation point from the ith source may be written

$$p_i^2 = \frac{\langle S_i \ p\rangle^2}{S_i^2} \quad . \tag{28}$$

Finally, the percentage contributed to the mean square pressure at the observation point by the ith source is given by

$$\% \equiv \frac{p_i^2}{p^2} = \frac{\langle S_i(t-\frac{\xi_i}{c}) \ p(t)\rangle^2}{\langle S_i^2(t)\rangle \ \langle p^2(t)\rangle} = C_{S_i p}^2(\tau_o) \tag{29}$$

where the right-hand side is observed to be equal to the square of the normalized cross-correlation between the source volume velocity and the observation point pressure evaluated at the retarded time delay $\tau_o = \xi_i/c$.

For a band limited random source the normalized crosscorrelation is given by

$$C_{S_i p}(\tau) = C_{S_i p}(\tau_o) \frac{\sin \pi B \ (\tau-\tau_o)}{\pi B \ (\tau-\tau_o)} \ \cos \omega_o(\tau-\tau_o) \tag{30}$$

where B is the source band width, ω_o is the source center frequency, and τ_o is the time delay, $\tau_o = \xi_i/c$. The normalized crosscorrelation consists of a cosine function oscillating at the center frequency of the excitation band modulated by a decaying sin x/x function which depends on the source bandwidth. The first side lobe in the correlation function occurs at a time delay of $\tau = 2\pi/\omega_o$. For octave band excitation the ratio of the first side lobe peak to the primary peak is .36 and for third octave band excitation the ratio is .9. Therefore filtering the source and receiver signal in octave bands allows some frequency resolution while still making it possible to identify the fundamental peak in the correlation function which occurs at the time delay appropriate to the acoustic wave travel time from the source to receiver.

From Eq. (30) we observe that the contribution E of reflected waves to the crosscorrelation at the time delay $\tau = \tau_o$ corresponding to the direct path transmission is given by

$$E = \frac{\sin \pi B (\Delta\tau_i)}{\pi B (\Delta\tau_i)} \tag{31}$$

where $\Delta\tau$ is the difference in propagation time from the source to receiver via the reflected and directed paths, i.e.,

$$\Delta\tau_i = \Delta\xi_i/c \tag{32}$$

where $\Delta\xi_i$ is the difference in path lengths between the reflected and direct paths.

In the application of this analysis to a wind tunnel problem we shall see that for octave band filtering of wide band random sources, the ratio given by Eq. (31) is very small so that the sound arriving at the observation point due to reverberation may indeed be viewed as noise. Of course the noise generated by wind flow over the microphone and by the tunnel air supply system is also uncorrelated with the test item sound. Therefore direct crosscorrelation of the source and receiver signals provides a means for determining the contribution of the direct path to the sound at the observation point.

Application of the crosscorrelation technique just discussed to the problem of determining the far field sound radiated by an aerodynamic source in a wind tunnel environment poses the problem of where to measure the source strength. In the case of rotating machinery, one possibility is to measure the fluctuating pressure on the blades; in the case of a jet engine exhaust, one might measure the fluctuating pressure at some point in the exhaust. However in these cases the source will generally encompass a number of independently radiating regions. The crosscorrelation coefficient discussed in the preceding analysis will reflect only the percentage of sound that comes from the correlated region immediately surrounding the source sensor.

Therefore using the correlation technique it is impossible to separate out the effects of multiple aerodynamic source regions from the degrading effects of reverberation. Fortunately, there is another analysis technique, namely coherency analysis which is ideally suited to determining the contribution of each aerodynamic source to the sound received at some far field point in the presence of reverberation.

We first demonstrate that for a linear time invariant system, reverberation does not effect the magnitude of the coherency between a source and receiver. Figure 14 illustrate the direct and reflected acoustic wave paths between the source A and receiver B located in reverberant space. For a linear time invariant system with no noise sources other than the one located at A the auto spectrum of the receiver signal is related to that of the source signal by

$$S_B(\omega) = |H_{AB}(\omega)|^2 S_A(\omega) \tag{33}$$

where H_{AB} is the frequency response function between the source and receiver. The cross spectrum between the source and receiver signals is

$$S_{AB}(\omega) = H_{AB}(\omega)S_A(\omega) \quad . \tag{34}$$

The coherency between the source and receiver γ_{AB} is defined as the magnitude squared of the cross spectrum divided by the product of the auto spectral densities of the source and receiver.

$$\gamma^2_{AB}(\omega) = \frac{|S_{AB}(\omega)|^2}{S_A(\omega)S_B(\omega)} = 1 \tag{35}$$

We have substituted the results from Eq. (33) and (34) into Eq. (35) to show that the coherence between the source and receiver signal is unity even in the presence of reverberation.

If one had an aerodynamic source located in a reverberant wind tunnel,the coherence between that source pressure and the pressure measured at a far field point in the tunnel would be unity even in the presence of reverberation. (We assume here that wind and tunnel noise are negligible.) Alternatively if a test item located in the wind tunnel involves a number of independent aerodynamic sources the coherence between one of these sources and the mean square pressure measured at a far field point can be interpreted as the percentage of the far field noise radiated by the source of interest. The correlation technique previously discussed could be used to determine the percentage of a far field pressure measurement due to reverberation and the percentage due to radiation from the test item. Then one could use coherency measurements to determine the contribution of each source of noise associated with the test item to the pressure received at the far field point.

These considerations suggest that combining crosscorrelation and coherency analyses may provide a means for measuring the directivity of an aerodynamic noise source located in a wind tunnel at a point far removed from the source. However this approach obviously needs further investigation.

Experiments

An electronic acoustic driver was placed in the center of the test section of the NASA Ames 40 x 80 ft wind tunnel and the voltage input to this driver was crosscorrelated with an acoustic signal measured at various distances from the source in order to determine the effects of tunnel reverberation, tunnel self noise, and wind noise on wind tunnel acoustic measurements. Figure 15 shows the test setup. The acoustic signal was measured at three measurement locations: .3, 4.5, and 13.5 meters from the source on the tunnel centerline. The acoustic signal was measured with three types of microphones; a 1/2-in. B & K microphone with a nose cone, a 3-ft AKG shotgun microphone, and a 6-in. BBN porous pipe microphone designed to discriminate against wind noise.

The acoustic driver was excited with octave bands of noise centered on 1000, 2000, and 4000 Hz. In each case the voltage into the driver was crosscorrelated with the acoustic signal. The normalized crosscorrelations evaluated at the time delay appropriate to the acoustic wave transmission from the source to the receiver are interpreted according to Eqs. (29) as the percentage of the sound measured at the receiver point attributable to the direct path from the acoustic driver.

Figure 16 shows a typical correlogram measured with the 1/2-in. B & K microphone located 4.5 m downstream of the source excited with octave band excitation centered at 2000 Hz with no wind. The measured correlogram has the appropriate decaying cosine form indicated by Eq. (30). The peaks in the crosscorrelation are separated by .5 milliseconds corresponding to the filter center frequency of 2000 Hz. The maximum correlation occurs at τ_0 = 0.0137 sec which is approximately equal to 4.5 meters divided by the speed of sound, c = 330 meters per sec. The maximum value of the crosscorrelation coefficient measured at the appropriate time delay is C_{max} = 0.71 indicating that approximately 1/2 of the mean square pressure measured at the

4.5 meter position, represents sound directly from the source and the other 1/2 represents mean square pressure associated with reverberation and tunnel background noise.

In this case the difference between the shortest reflection path involving the tunnel ceiling and the direct path is approximately 8.1 meters so that the first reflected wave would arrive approximately 25 milliseconds after the direct wave. From Eq. (31) the correlation between the first reflection and the source signal at the time delay appropriate to the direct path is approximately 10^{-10}, confirming at least in this example that the reverberant signals do not contribute to the crosscorrelation evaluated at the direct path time delay.

Tables V, VI, and VII show the maximum values of the normalized crosscorrelation between microphone outputs and the speaker input for microphones located 13.5 meters, 4.5 meters, and .3 meters downstream of the speaker respectively.

Referring to the data presented in Table V for the microphone located 13.5 meters downstream of the speaker, the maximum correlation measured at 1000 Hz with the 1/2-in. microphone for no wind was .38 indicating that $.38^2$ or 1/7 of the mean-square pressure arriving at the microphone was due to the direct

Table V - Maximum Values of Correlation Between Microphone Output And Speaker Input With Microphones 13.5m Downstream of Speaker

Frequency (Hz)	Function	No Wind			Wind		
		½-in. B & K	Shot Gun	Porous	½-in. B & K	Shot Gun	Porous
1000	C_{max}	.38	.58	.58	.30	.30	.30
	τ_m(msec)	41	42	41	38	39	39
2000	C_{max}	.55	.75	.75	.43	.65	.79
	τ_m(msec)	41	42	41	38	39	38
4000	C_{max}	.55	.63	.70	.55	.73	.50
	τ_m(msec)	41	42	41	38	39	38

Table VI - Maximum Values of Correlation Between Microphone Output And Speaker Input With Microphones <u>4.5m</u> Downstream of Speaker

Frequency (Hz)	Function	No Wind			Wind		
		½-in. B & K	Shot Gun	Porous	½-in. B & K	Shot Gun	Porous
1000	C_{max}	.83	.85	.85	.60	.70	.75
	τ_m(msec)	14	15	14	13	14	13
2000	C_{max}	.71	.88	.90	.75	.88	.90
	τ_m(msec)	14	15	14	13	14	13
4000	C_{max}	.88	.80	.88	.75	.78	.85
	τ_m(msec)	14	15	14	13	14	13

Table VII - Maximum Values of Correlation Between Microphone Output And Speaker Input With Microphones .3m Downstream of Speaker

Frequency (Hz)	Function	No Wind		Wind	
		½-in. B & K	Shot Gun	½-in. B & K	Shot Gun
1000	C_{max}	.90	.95	.60	.87
	τ_m(msec)	1.6	3	1.3	2.6
2000	C_{max}	.87	.87	.75	.86
	τ_m(msec)	1.6	3	1.3	2.6
4000	C_{max}	.87	.80	.87	.83
	τ_m(msec)	1.6	3.3	1.2	2.6

field. This measurement is in agreement with the direct and reverberant field measurements in the 40 x 80 ft tunnel presented in Fig. 17.[2/] That data shows that the direct field is 8 dB down from the reverberant field, 13.5 meters downstream of an omnidirectional source at 1000 Hz. The shotgun and porous pipe microphone resulted in correlations of .58 at 1000 Hz with no wind, indicating that the directionality of these microphones tended to discriminate against reverberation.

With wind the correlation measured at 1000 Hz falls to .3 for all microphones, which indicates that only 10% of the mean-square pressure at the microphone is due to the direct acoustic field. At frequencies of 2000 and 4000 Hz, the use of the shotgun and porous pipe microphones again resulted in higher correlations than the 1/2-in. microphone. With wind at 2000 and 4000 Hz, the shotgun and porous pipe microphones resulted in significant improvement. The time delay for maximum cross correlation is approximately 41 milliseconds which is equal to the travel distance 13.5 meters divided by the speed of sound. The introduction of wind with velocity 16.5 meters/sec in the tunnel reduced the time for a maximum crosscorrelation by approximately 5%.

Figure 18 shows a plot of some of the data presented in Table V for the 13.5 meter microphone position. The open circles and squares represent data measured with the 1/2-in. B & K and the 3-ft shotgun microphone respectively with no wind, and the closed symbols indicate the same measurements in the presence of wind. Note that at the higher frequencies 2000 and 4000 Hz, the 3-ft shotgun microphone provided reasonably large correlation even in the presence of wind. It is anticipated that the use of even more directional microphones would result in higher crosscorrelation in the low frequency bands.

These preliminary results indicate that the feasibility of using crosscorrelation measurements to measure the direct radiation field of a single acoustic source in a reverberant wind tunnel environment. A more complete table of crosscorrelation data for various frequencies and microphone locations should be compiled. This catalog of data could be used to correct for the degrading effects of reverberation, tunnel background noise, and wind microphone noise in measurements of the crosscorrelation between the source pressures and radiated pressures in flight vehicle tests.

In the flight vehicle tests the source pressures would be measured on the surface of helicopter rotors or fan blades, in the exhaust of jet engines, and on blown flap surfaces. When those data are corrected using this catalog, the data would indicate the percentage of the sound at that receiver point radiated from the source measurement point. Of course, the corrections will involve the directionality characteristics of the source, since a source oriented with the major directivity lobe pointing directly along the axis of the tunnel will result in a higher ratio of direct to reverberant sound than one whose major radiation lobe is oriented perpendicular to the axis of the tunnel. Therefore the catalog would necessarily have to include measurements for electronic speakers with various directivity patterns.

CONCLUSIONS

The following conclusions regarding the relationship between the near field and far field of a typical acoustic source in a wind tunnel environment are deduced from this investigation.

1. The geometric near field generally extends further from the test item than the hydrodynamic near field.

2. In a hardwall tunnel, directionality measurements are usually possible in the geometric near field but are not possible, without resorting to special techniques, in the far field because of the degrading effects of reverberation.

3. Analytical techniques for calculating the far field directivity on the basis of near field acoustic data do not appear promising.

4. Directionality data measured in the geometric near field of typical test items may represent reasonable approximations to the far field directivity.

5. Crosscorrelation experiments conducted with simple acoustic drivers would provide a means for quantifying the effects of reverberation and wind noise on directionality measurements.

6. Coherency analyses are preferable to crosscorrelation analyses for determining the relationship between radiated acoustic pressures and source aerodynamic pressures, because reverberation does not reduce coherency.

REFERENCES

1. D. Hickey, P. T. Soderman, and M. Kelly, "Noise Measurements in Wind Tunnels," NASA SP-207, p. 399-408, July 1969.

2. D. A. Bies, "Investigation of the Feasibility of Making Model Acoustic Measurements in the NASA Ames 40- By 80-Foot Wind Tunnel," BBN Report 1870, NASA CR-114352, 1970.

3. A. Atencio, Jr. and P. T. Soderman, "Comparison of Aircraft Noise Measured in Flight Test and in the NASA Ames 40- by 80-Foot Wind Tunnel, AIAA Paper No. 73-1047, October 1973.

4. A. Atencio, Jr., V. Kirk, P. T. Soderman, and L. P. Hall, "Comparison of Flight and Wind Tunnel Measurements of Jet Noise for the XV-5B Aircraft," NASA TMX-62, 182, NASA Ames Research Center, October 1972.

5. J. L. Butler, "A Series Expansion Method for the Prediction of the Far Field from Near Field Measurements," Parke Mathematical Laboratories, Inc., Scientific Report No. 1, 1968.

6. J. L. Butler, "A Method for the Prediction of the Far Field from Near Field Measurements of the Amplitude Alone," Parke Mathematical Laboratories, Inc., Scientific Report No. 3, 1969.

7. D. U. Noiseux, "Study of Porous Surface Microphones for Acoustic Measurements in Wind Tunnels," BBN Report 2539, NASA CR-114593, April 1973.

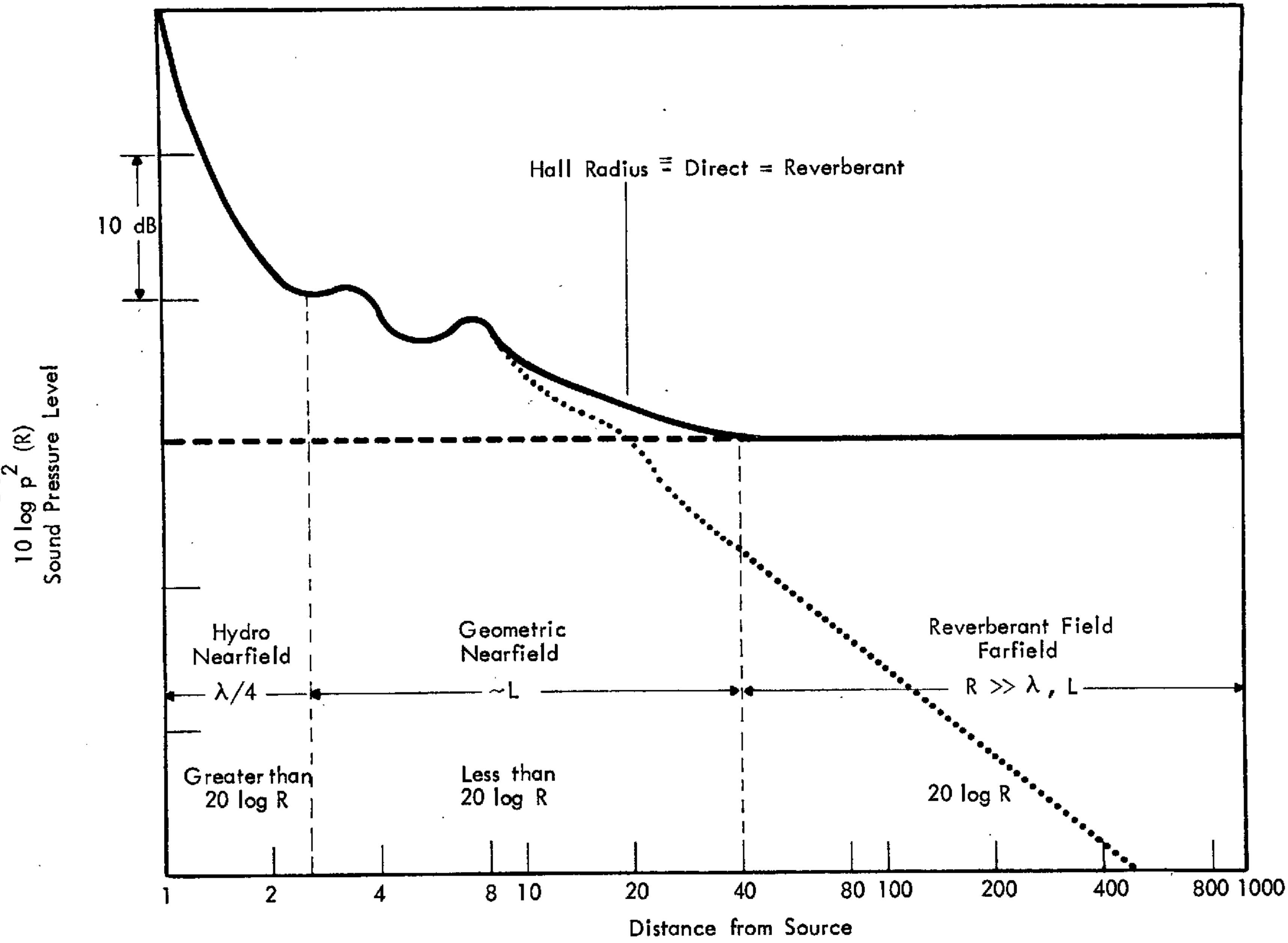

FIGURE 1. NEARFIELD AND FARFIELD DEFINITION

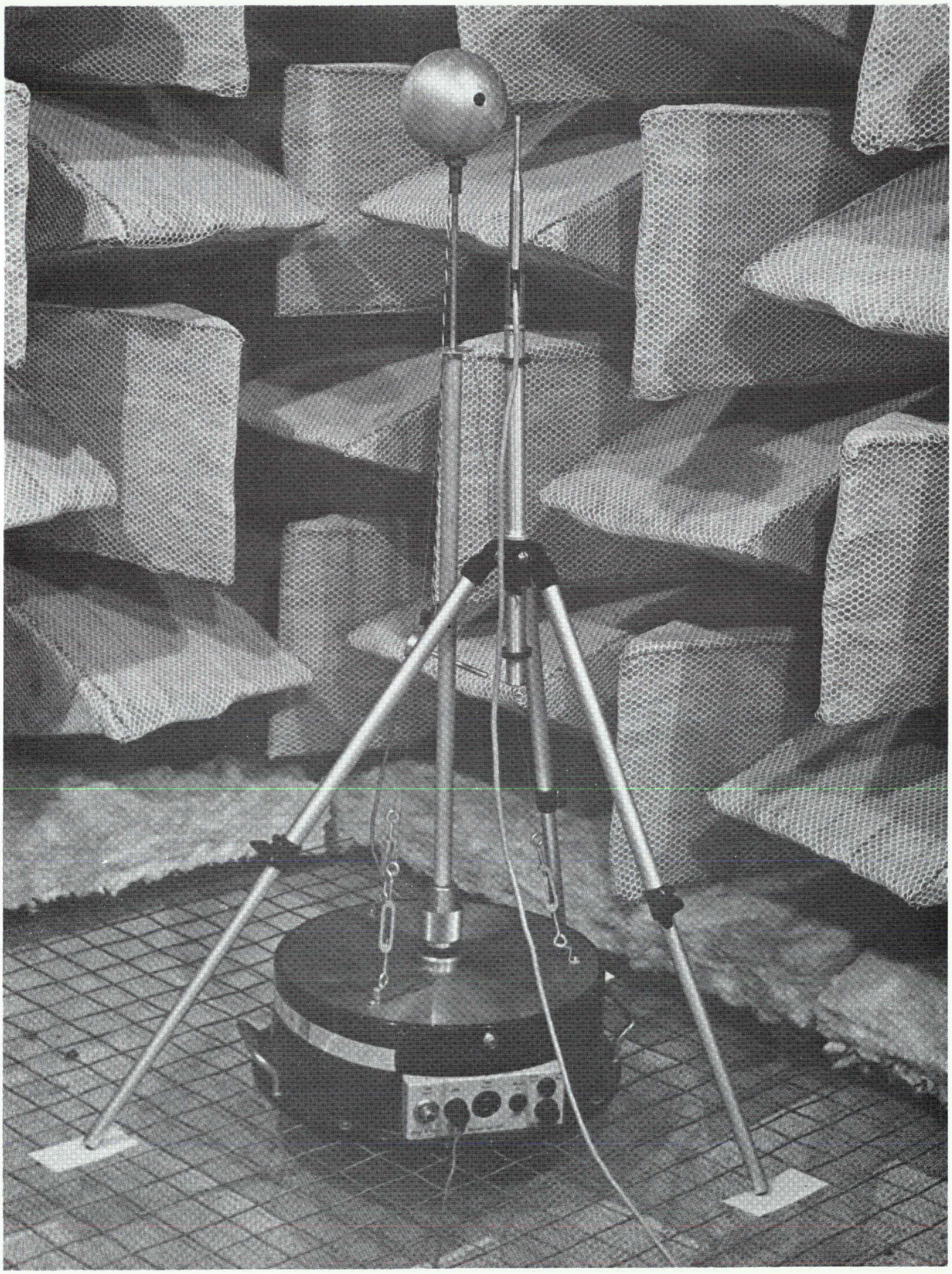

FIGURE 2. 10 cm DIAMETER SPHERICAL ACOUSTIC SOURCE LOCATED IN ANECHOIC CHAMBER

This page is reproduced at the back of the report by a different reproduction method to provide better detail.

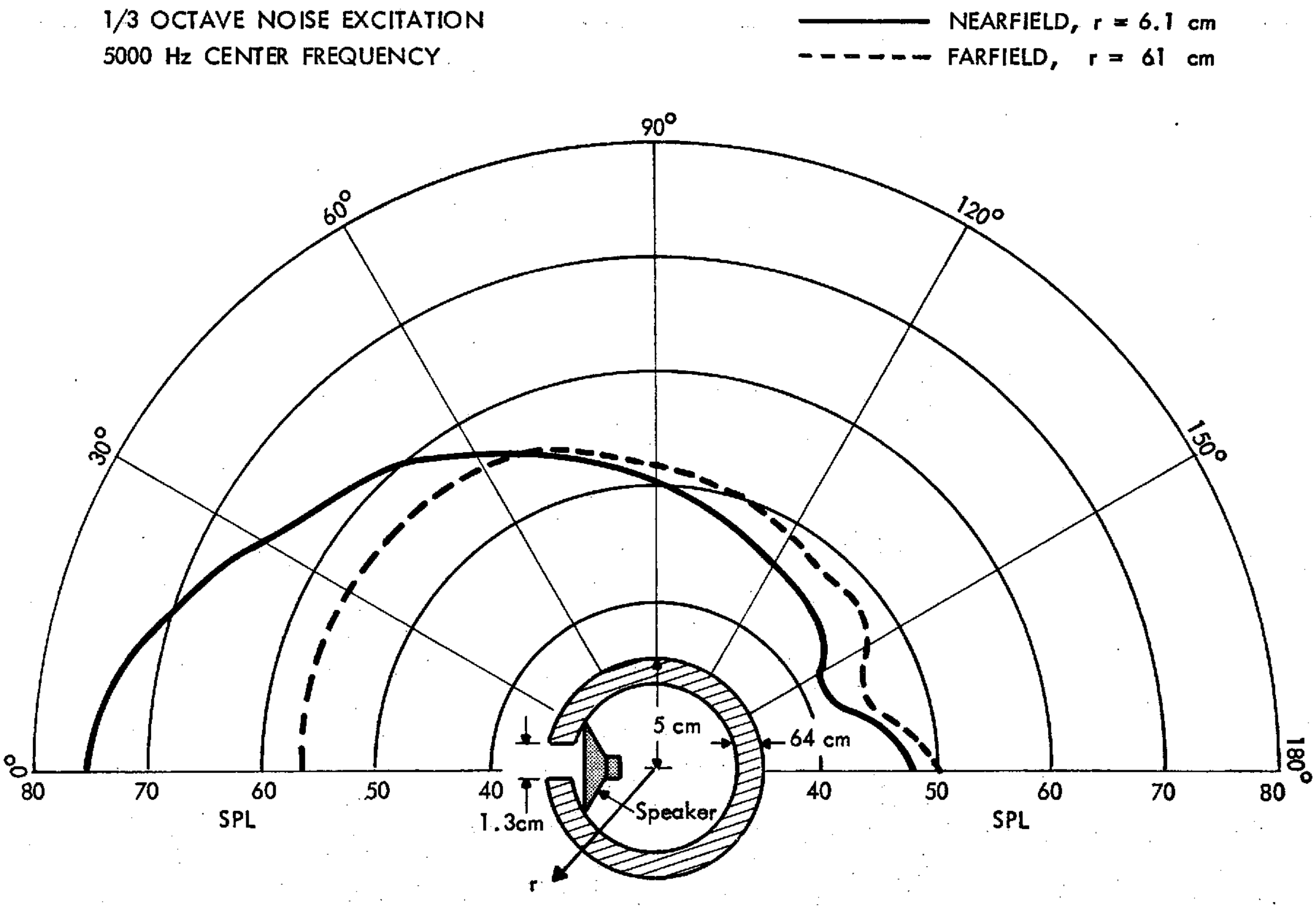

FIGURE 3. COMPARISON OF NEARFIELD AND FARFIELD ACOUSTIC DIRECTIONALITY MEASUREMENTS FOR A SIMPLE ACOUSTIC SOURCE LOCATED IN AN ANECHOIC ROOM

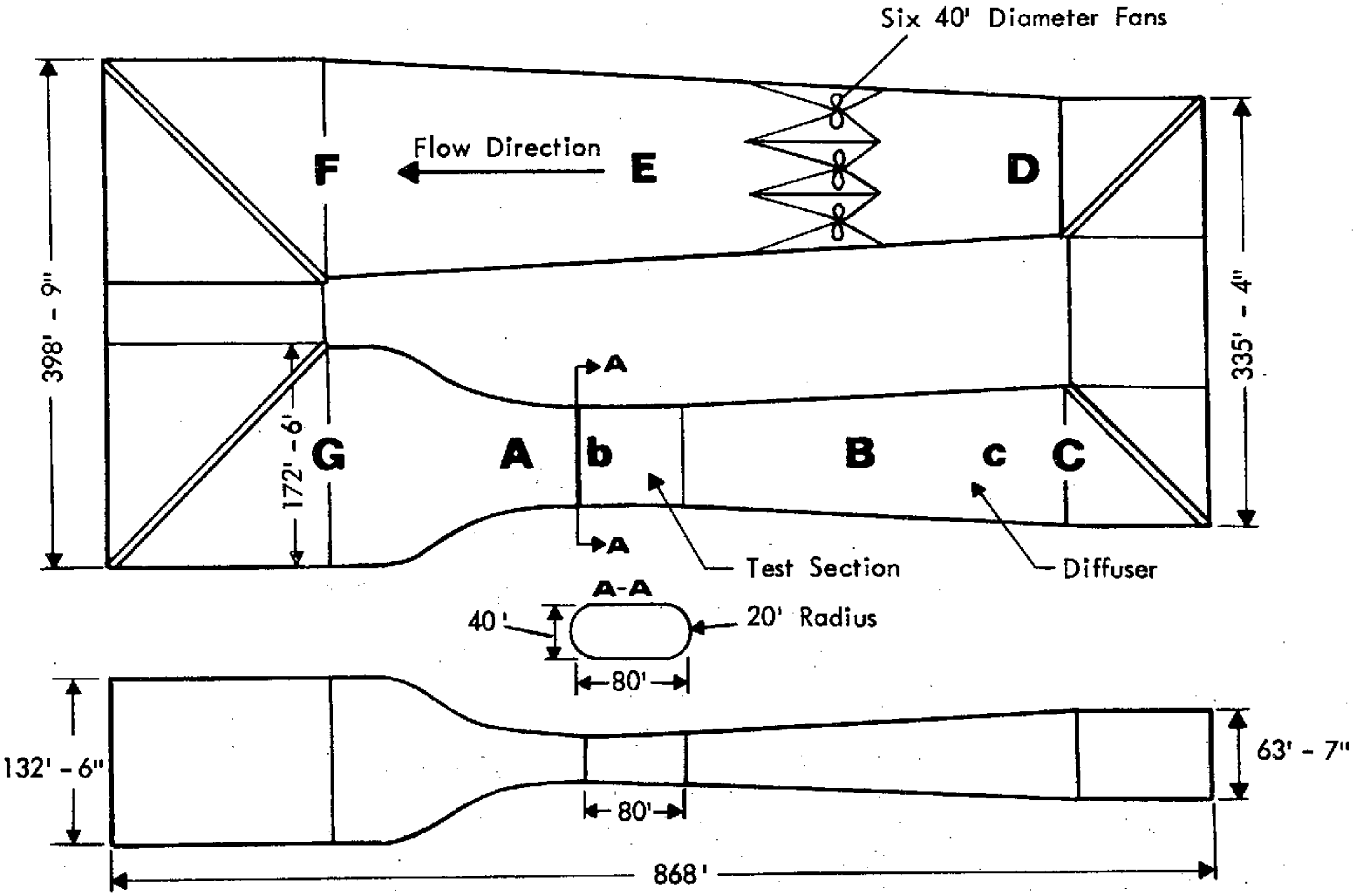

FIGURE 4. NASA AMES 40 FT. x 80 FT. WIND TUNNEL

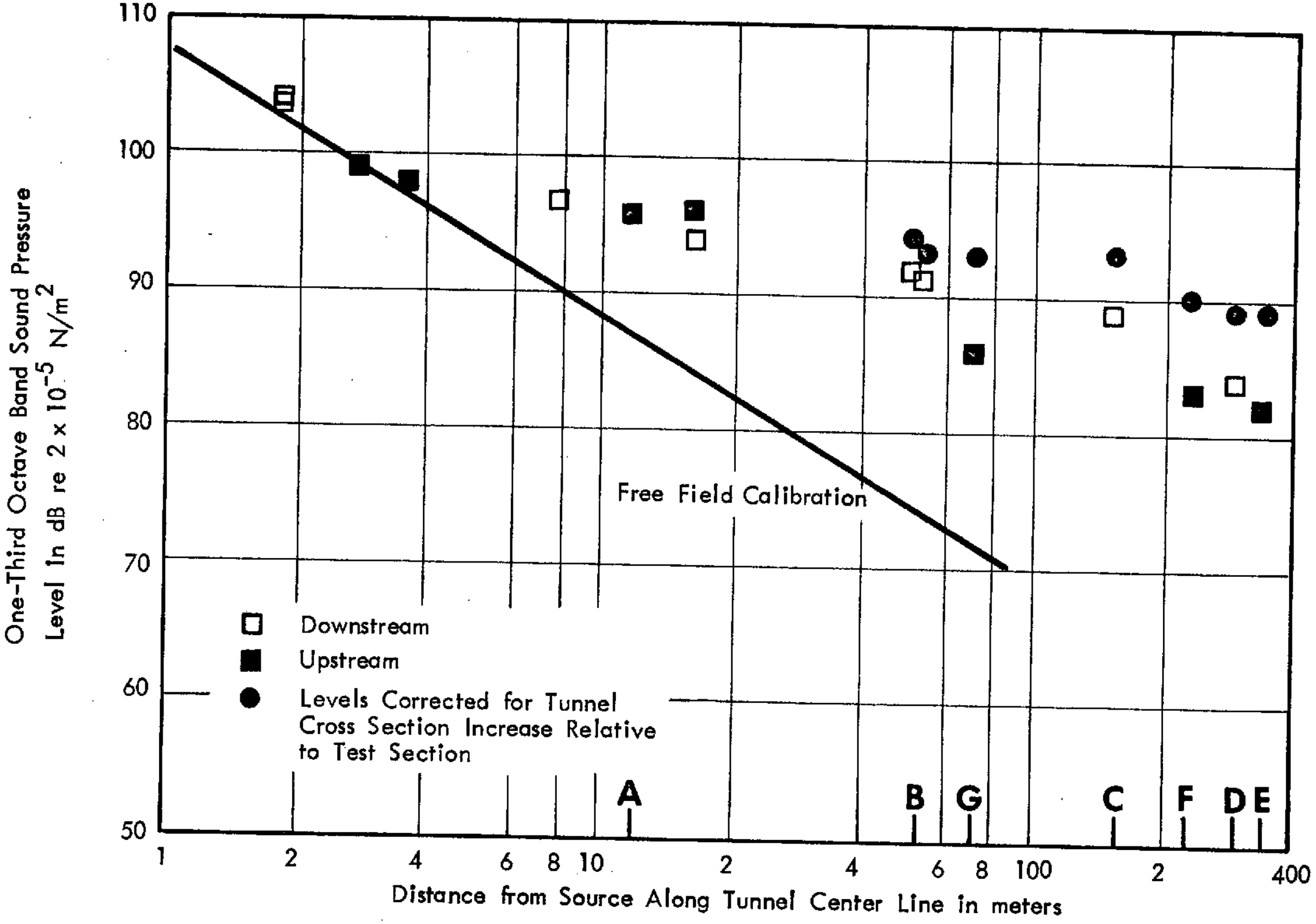

FIGURE 5. TUNNEL SOUND PRESSURE LEVELS DUE TO A DODECAHEDRON SOUND SOURCE IN THE TEST SECTION, 250 Hz 1/3 OCTAVE BAND, SOUND POWER LEVEL 119.5 dB RE 10-12 WATTS

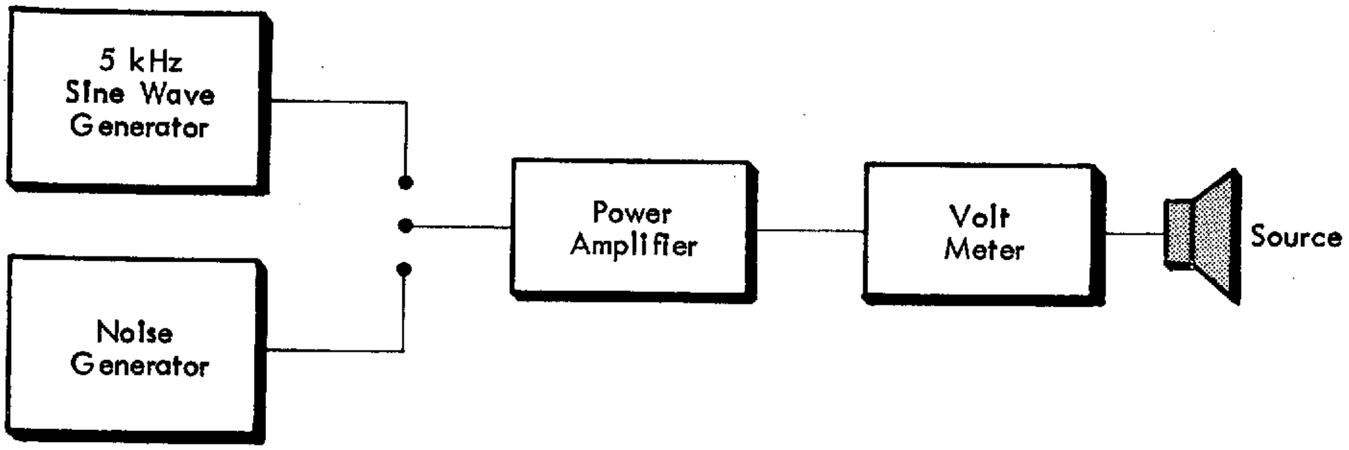

EXCITATION SYSTEM

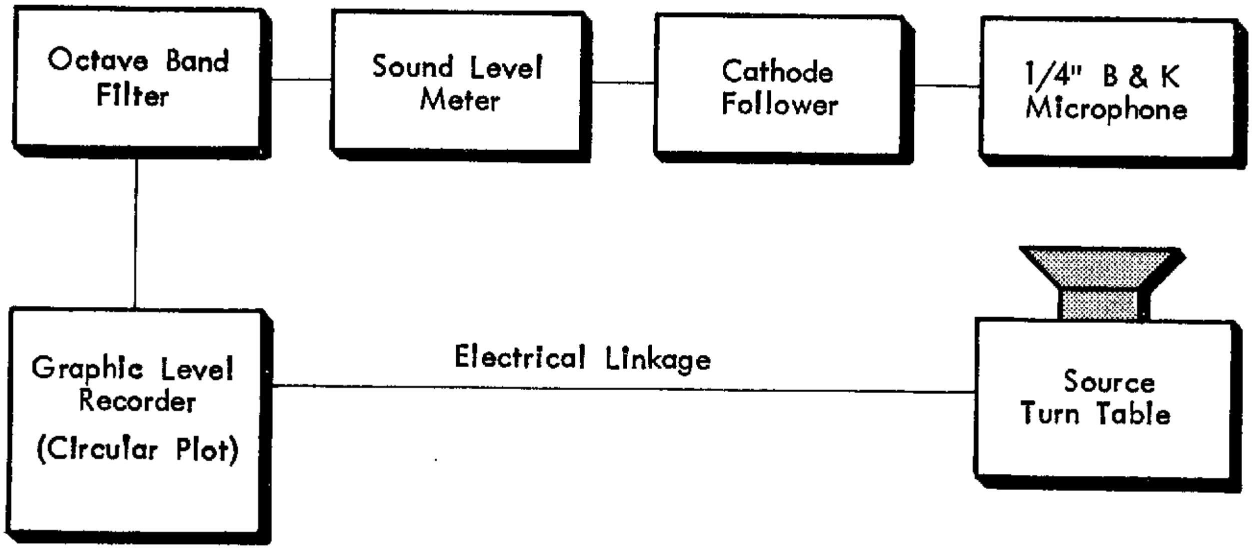

DETECTION SYSTEM

FIGURE 6. INSTRUMENT SET-UP IN ANECHOIC ROOM
SMALL SOURCE EXPERIMENTS

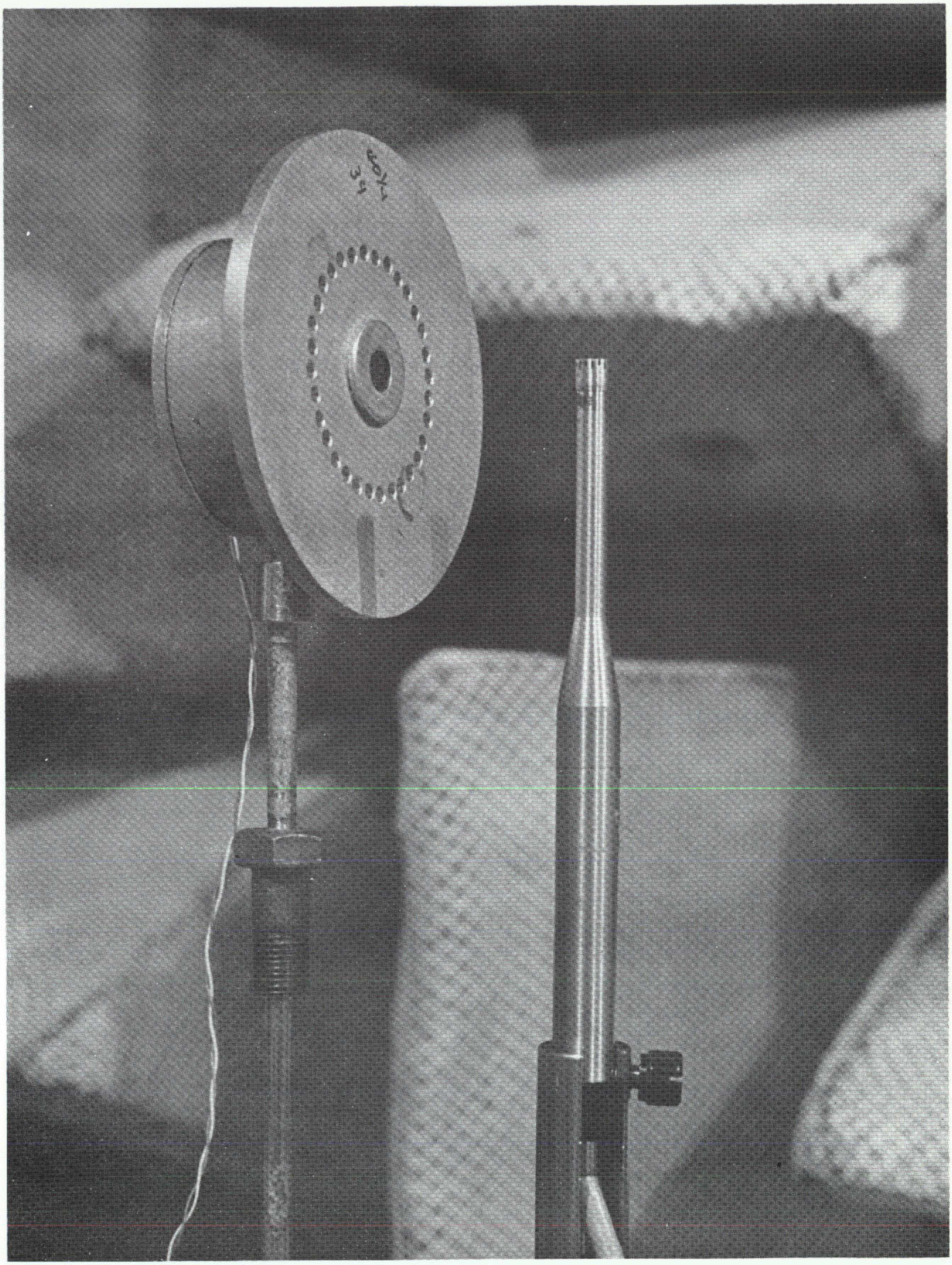

FIGURE 7. 15.84 cm DIAMETER LOLLIPOP ACOUSTICAL SOURCE AND MICROPHONE

This page is reproduced at the back of the report by a different reproduction method to provide better detail.

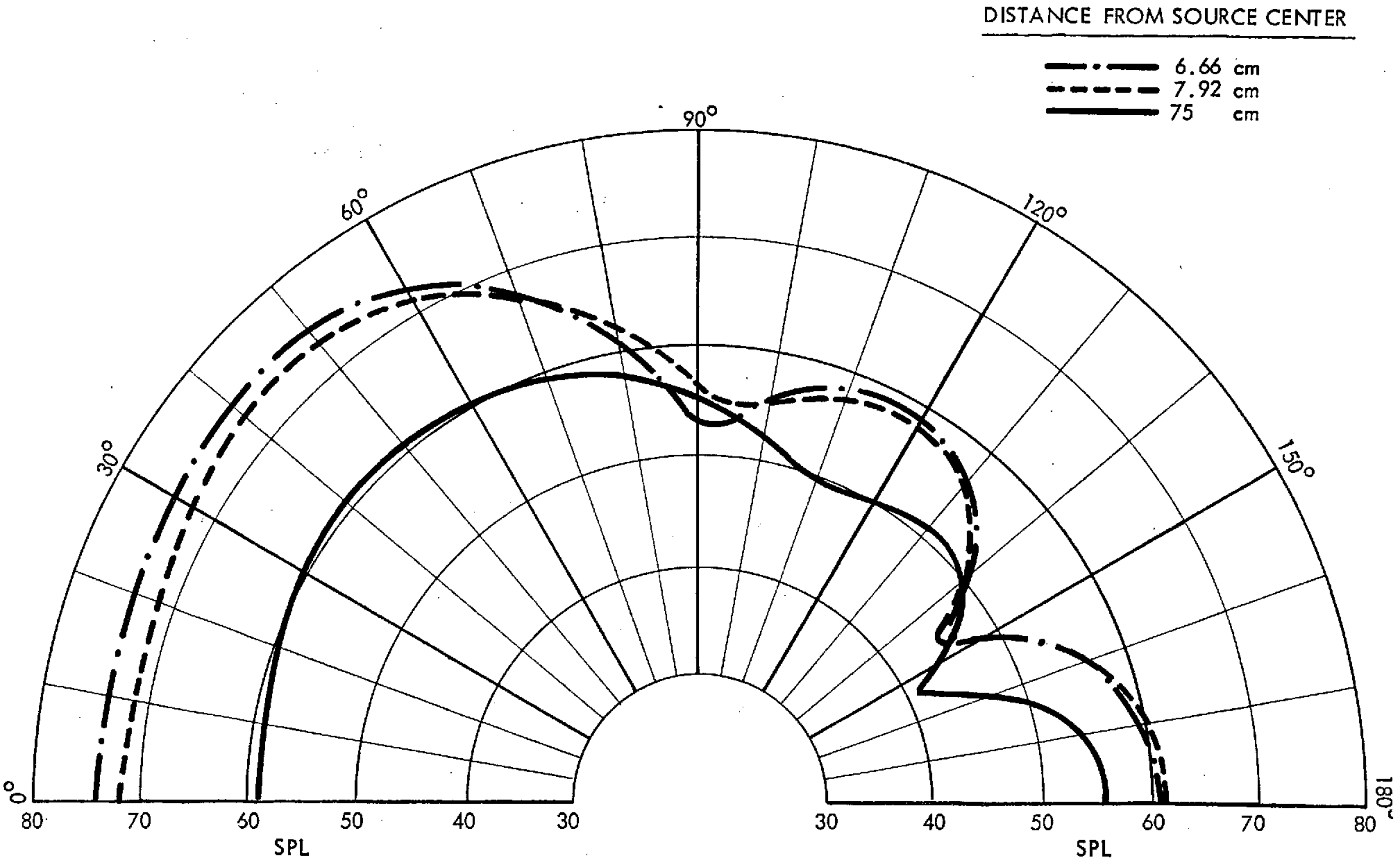

FIGURE 8. NEARFIELD AND FARFIELD SPL DATA FOR LOLLIPOP SOURCE -- 5 kHz PURE TONE EXCITATION (.3 Volts rms)

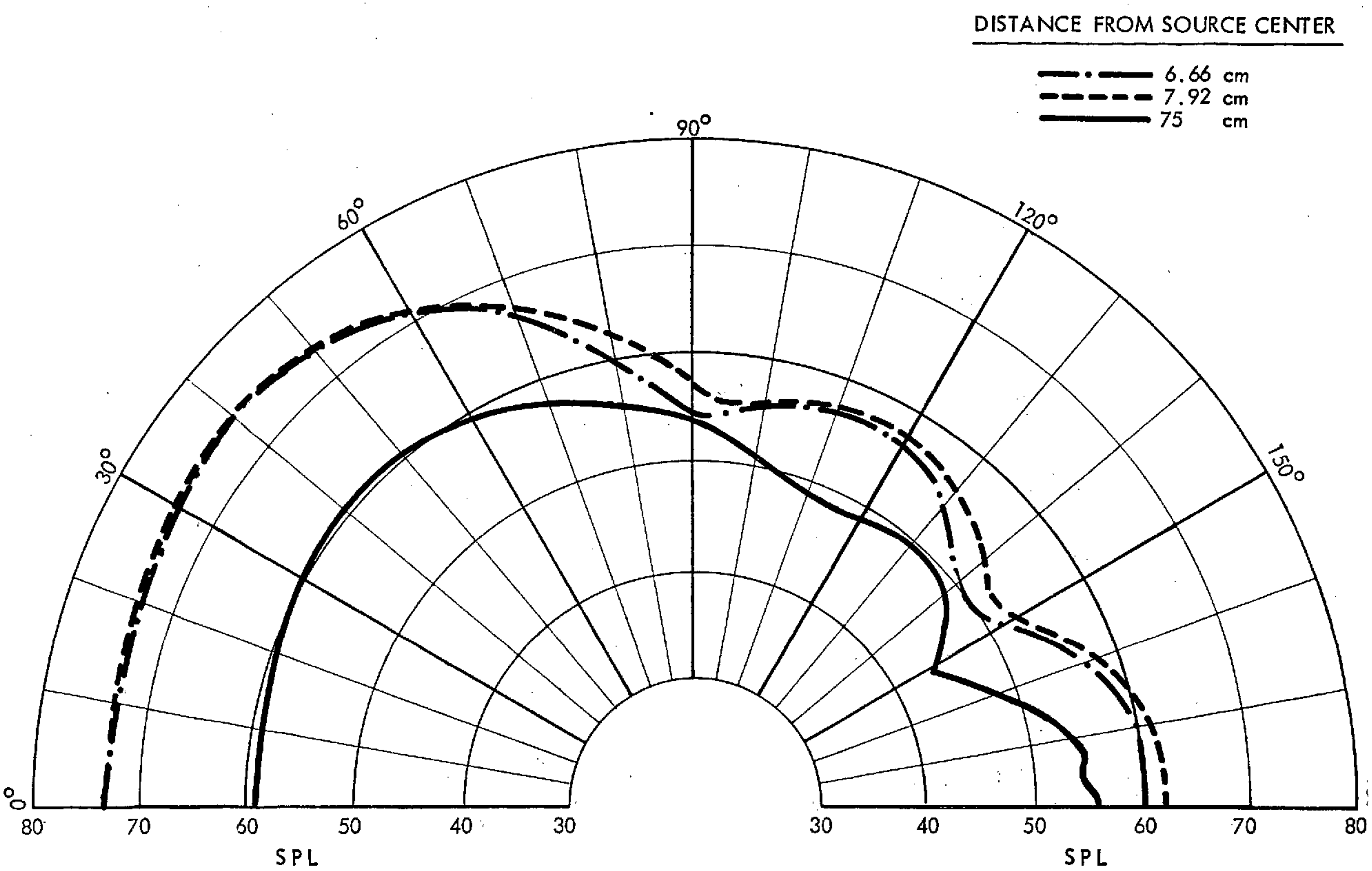

FIGURE 9. NEARFIELD AND FARFIELD SPL DATA FOR LOLLIPOP SOURCE -- 5 kHz, 1/10 OCTAVE BAND EXCITATION (.3 Volts rms)

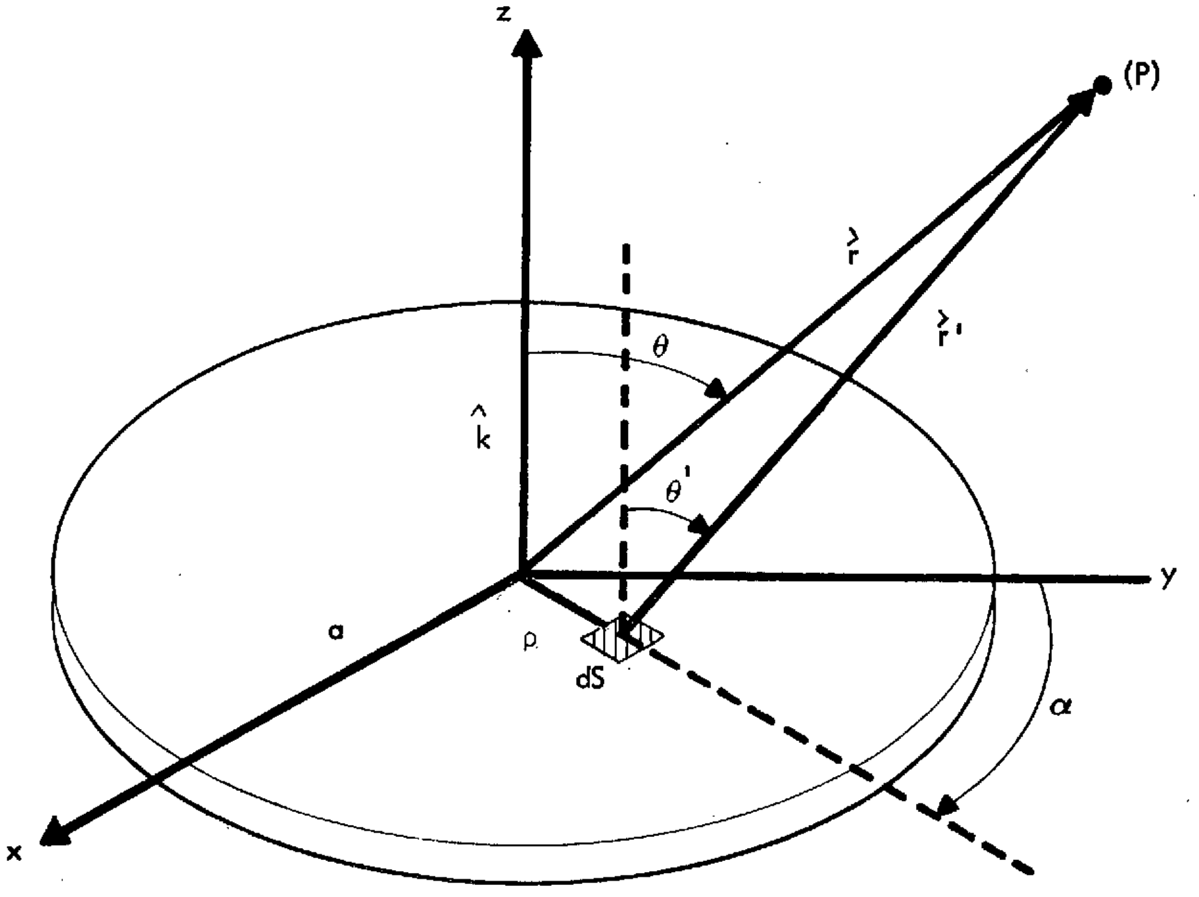

FIGURE 10. GEOMETRY FOR ANALYZER ERRORS ASSOCIATED WITH NEARFIELD MEASUREMENTS

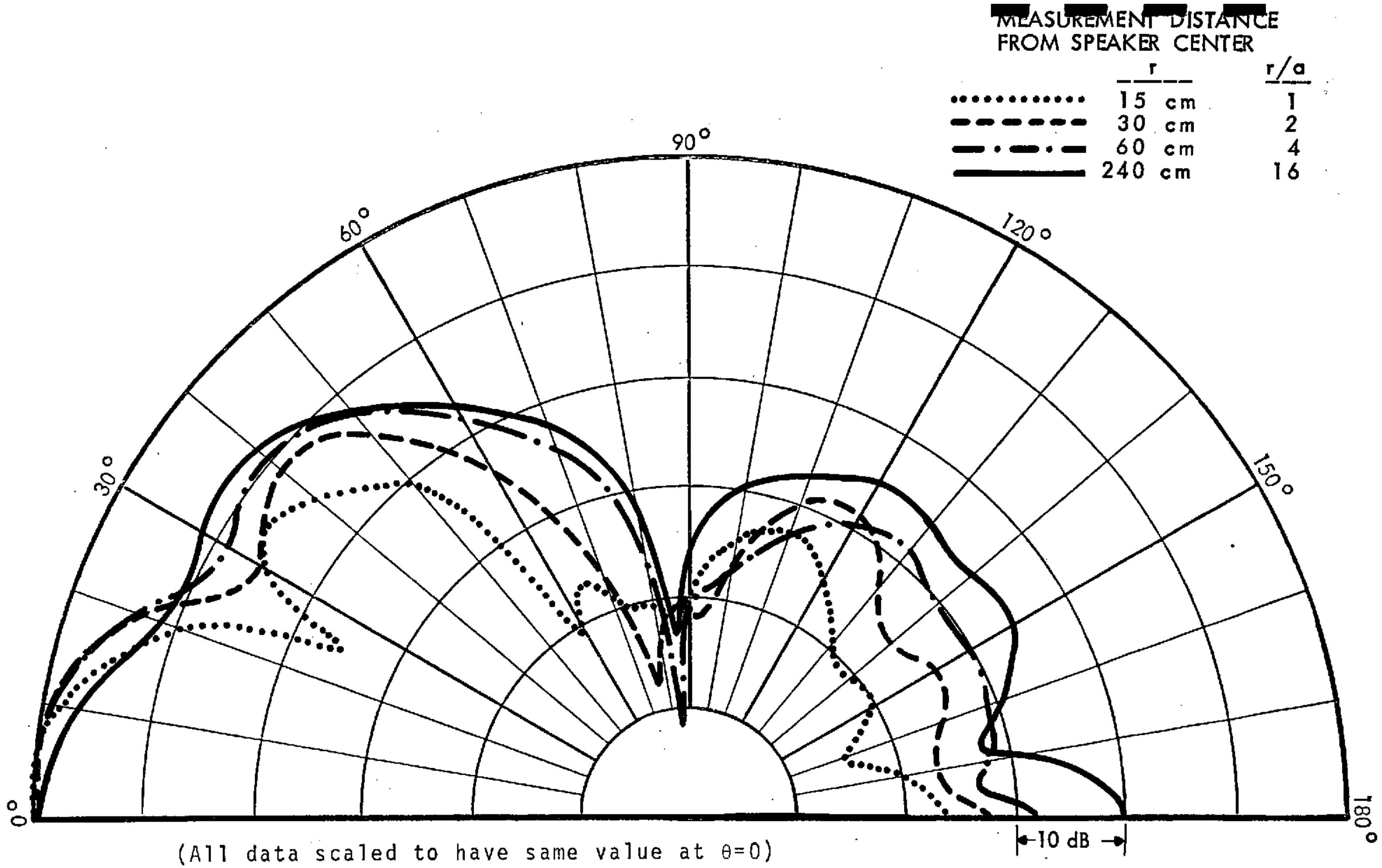

(All data scaled to have same value at θ=0)

FIGURE 11. DIRECTIONALITY PLOTS MEASURED WITH 1/2 INCH MICROPHONE AT VARIOUS DISTANCES FROM AN UNBAFFLED SPEAKER, a = 15 cm IN RADIUS (EXCITED WITH 1/3 OCTAVE BAND NOISE CENTERED AT 4000 Hz)

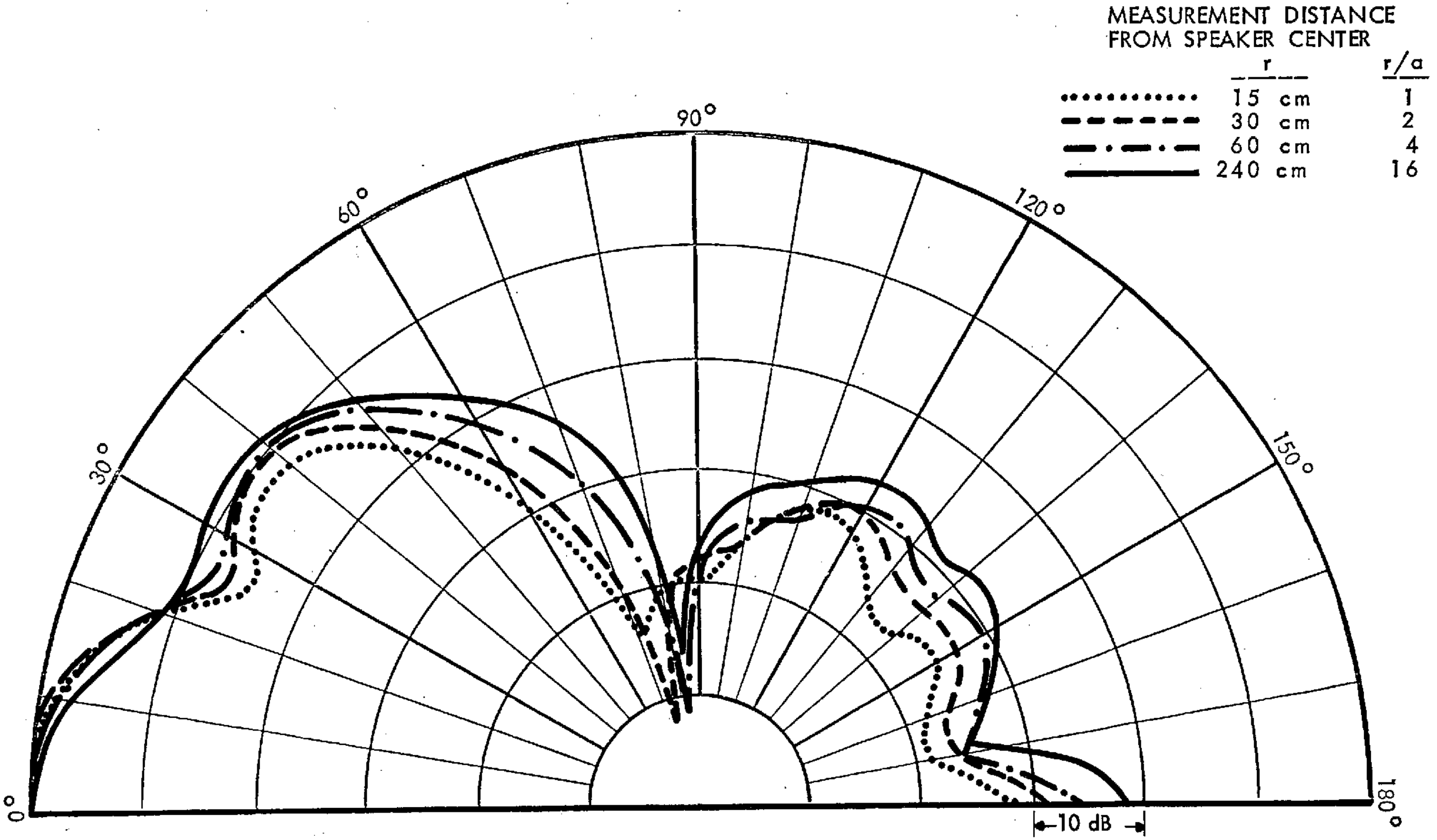

(All data scaled to have same value at $\theta=0$)

FIGURE 12. DIRECTIONALITY PLOTS MEASURED WITH POUROUS PIPE DIRECTIONAL MICROPHONE AT VARIOUS DISTANCES FROM AN UNBAFFLED SPEAKER, a = 15 cm IN RADIUS
(EXCITED WITH 1/3 OCTAVE BAND NOISE CENTERED AT 4000 Hz)

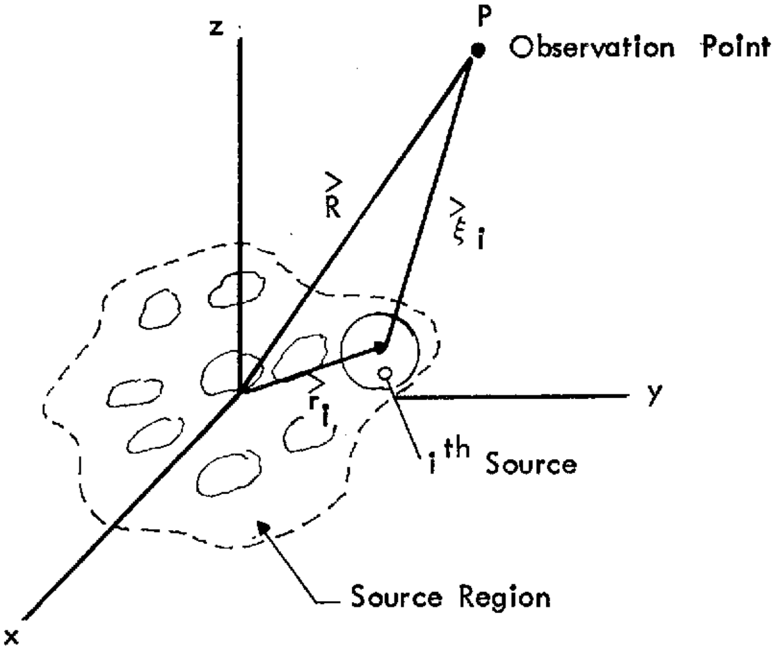

FIGURE 13. COORDINATE SYSTEM FOR CROSSCORRELATION ANALYZER

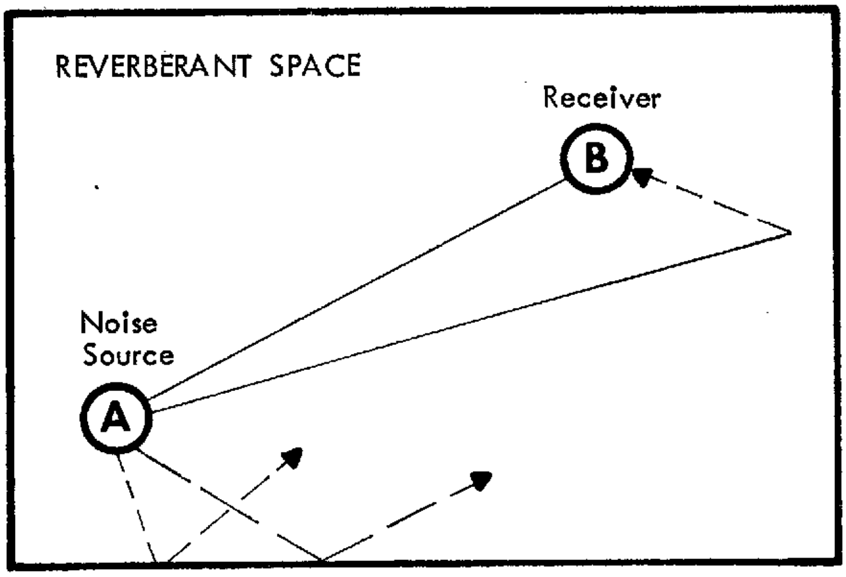

FIGURE 14. DIRECT AND REFLECTED PATHS BETWEEN SOURCE (A) AND RECEIVER (B)

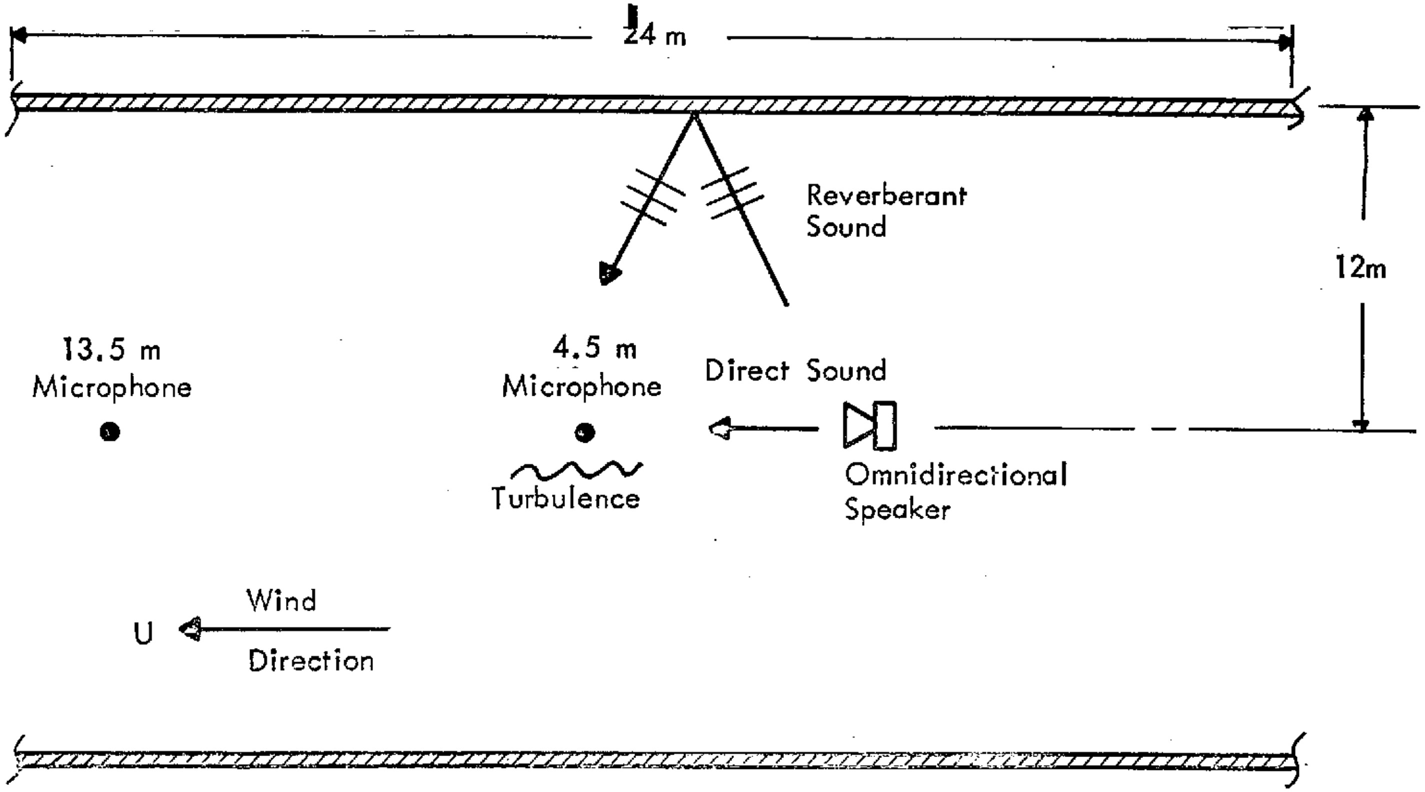

FIGURE 15A. SPEAKER AND MICROPHONE SET-UP IN WIND TUNNEL TEST SECTION

Type of Microphone	Distance Downstream of Source (d)		
1/2 in. B & K	.3 m	4.5 m	13.5 m
3 ft AKG Shotgun	.3 m	4.5 m	13.5 m
1 ft BBN Pourous Pipe		4.5m	13.5m

FIGURE 15 B. LOCATION OF MICROPHONES

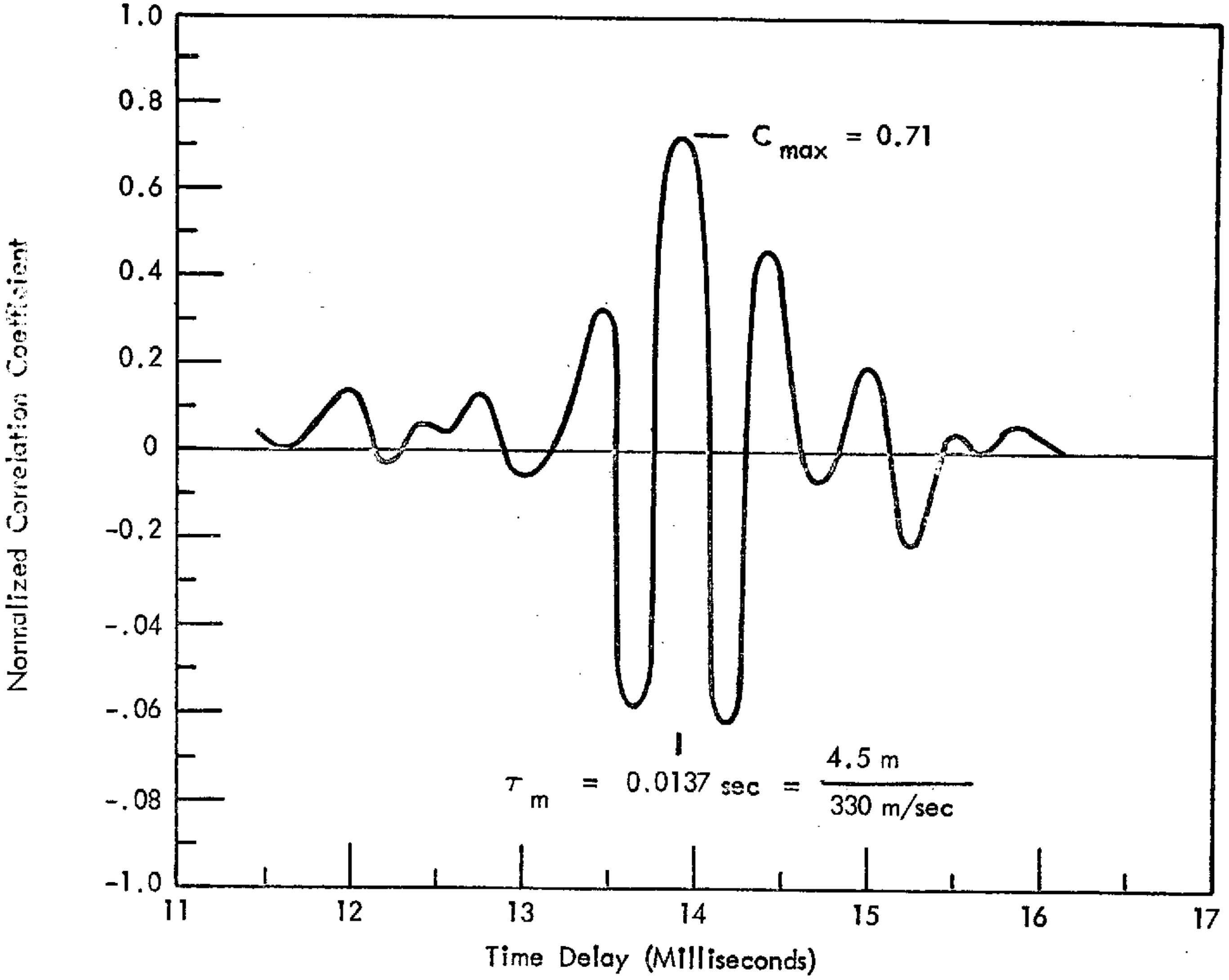

FIGURE 16. MEASURED NORMALIZED CROSSCORRELATION FOR 1/2 INCH B & K. MICROPHONE LOCATED 4.5 m DOWNSTREAM OF SOURCE EXCITED WITH OCTAVE BAND NOISE CENTERED AT 2000 Hz, NO WIND

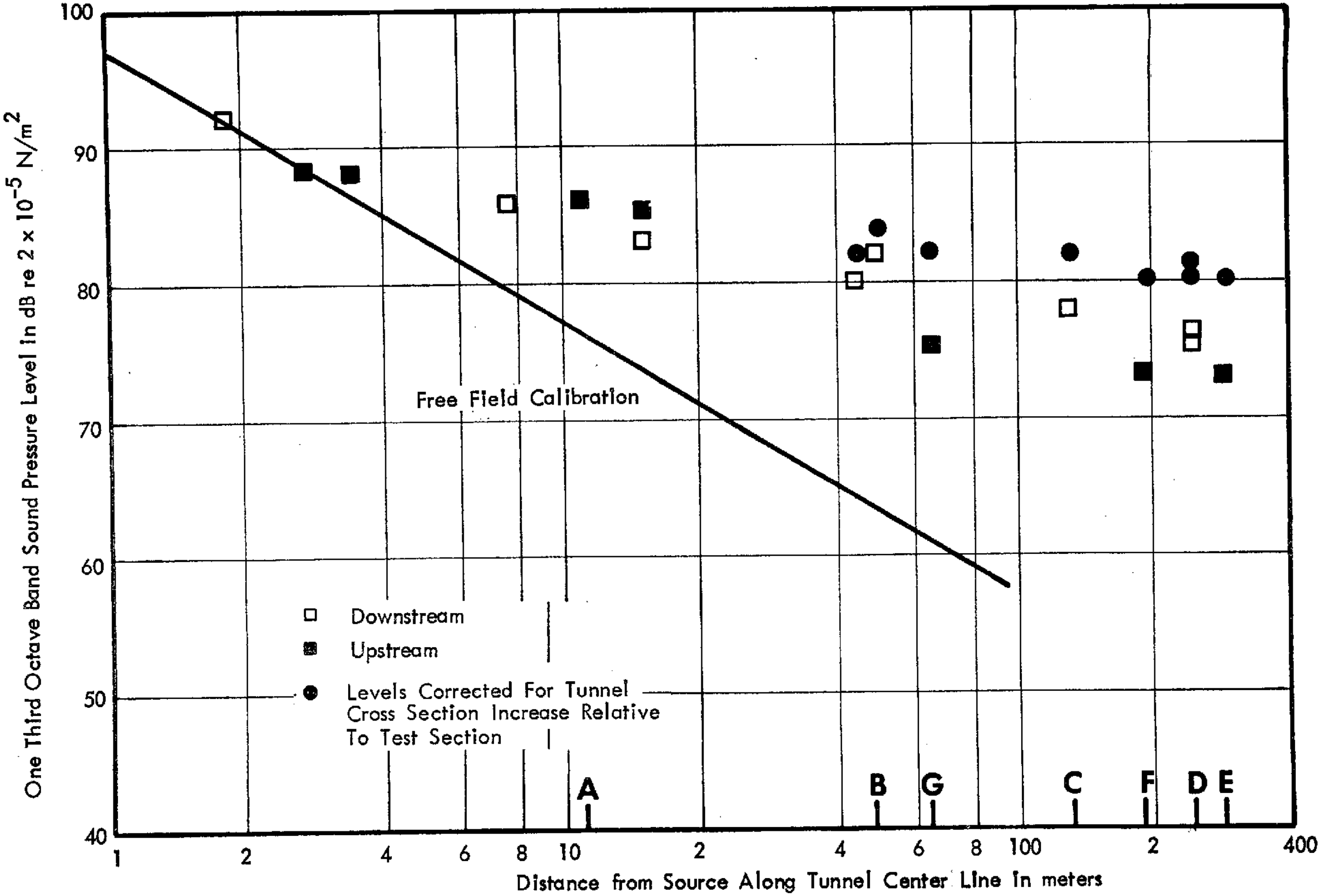

FIGURE 17. TUNNEL SOUND PRESSURE LEVELS DUE TO A DODECAHEDRON SOUND SOURCE IN THE TEST SECTION, 1000 Hz 1/3 OCTAVE BAND, 12 VOLTS RMS INPUT, SOUND POWER LEVEL 109.5 dB RE 10^{-12} VOLT

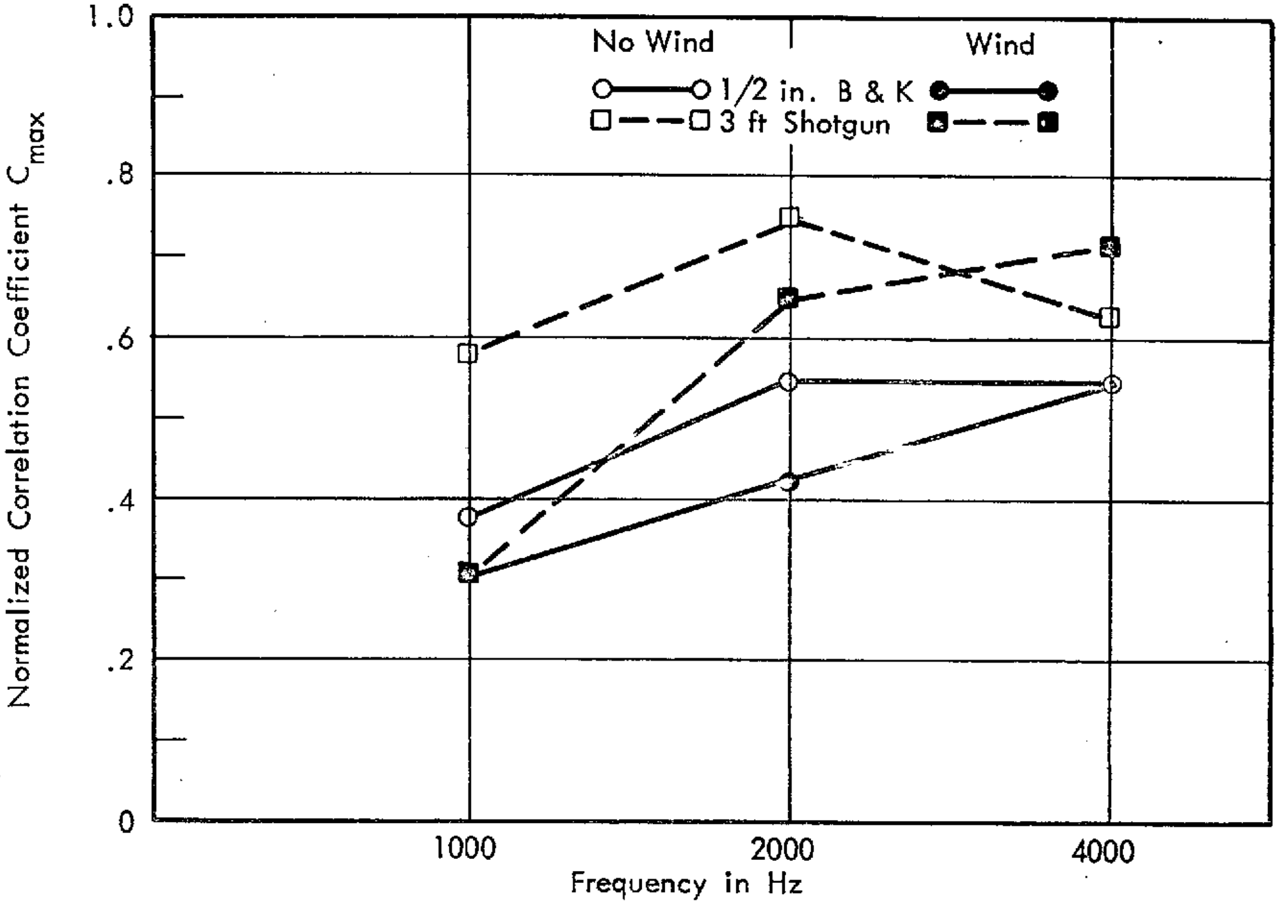

FIGURE 18. CORRELATIONS MEASURED AT 13.5 m WITH 1/2 IN. B & K AND 3 FT. SHOTGUN MICROPHONES

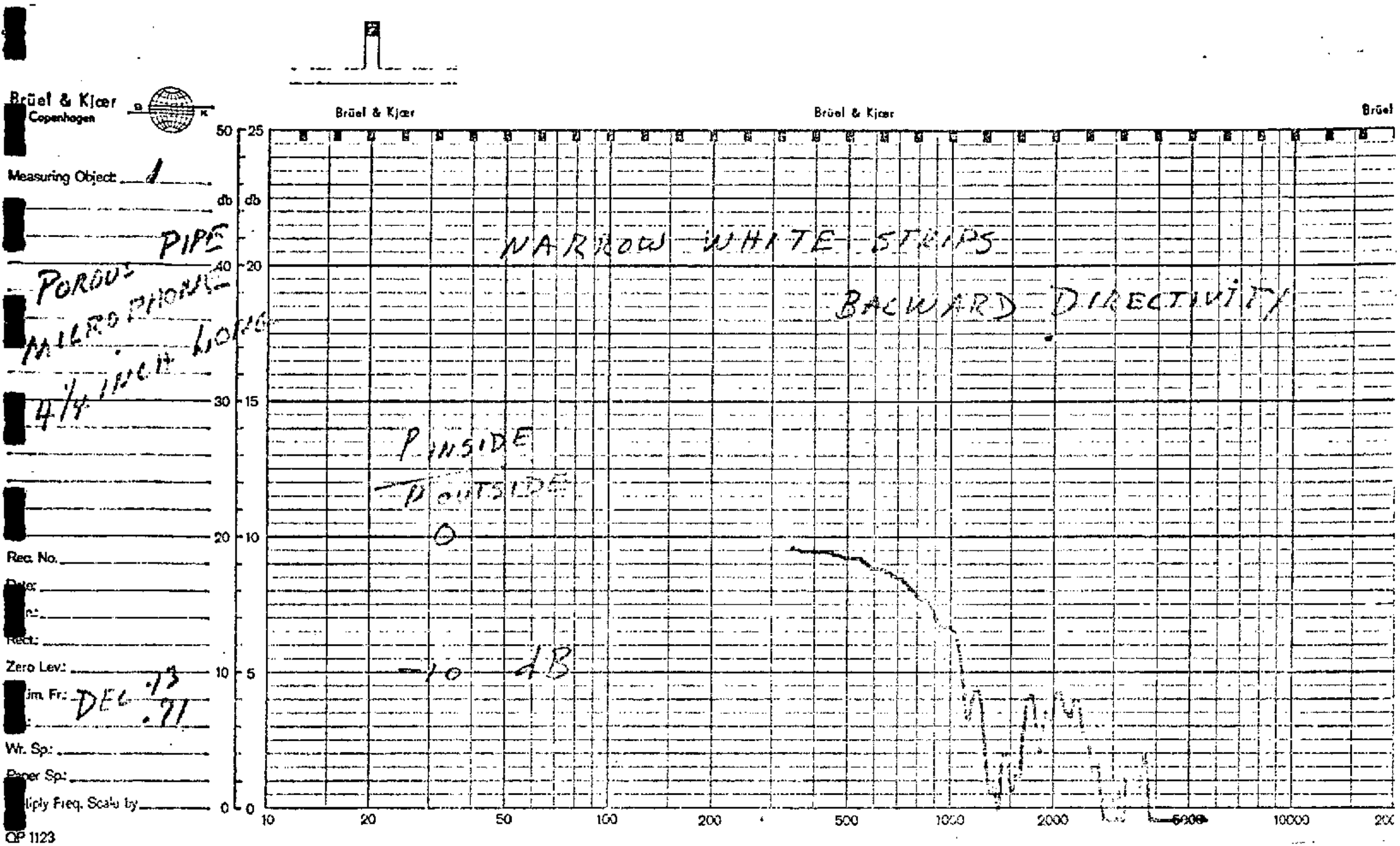

FIGURE A-1. BACKWARD DIRECTIVITY OF NARROW STRIPE MICROPHONE

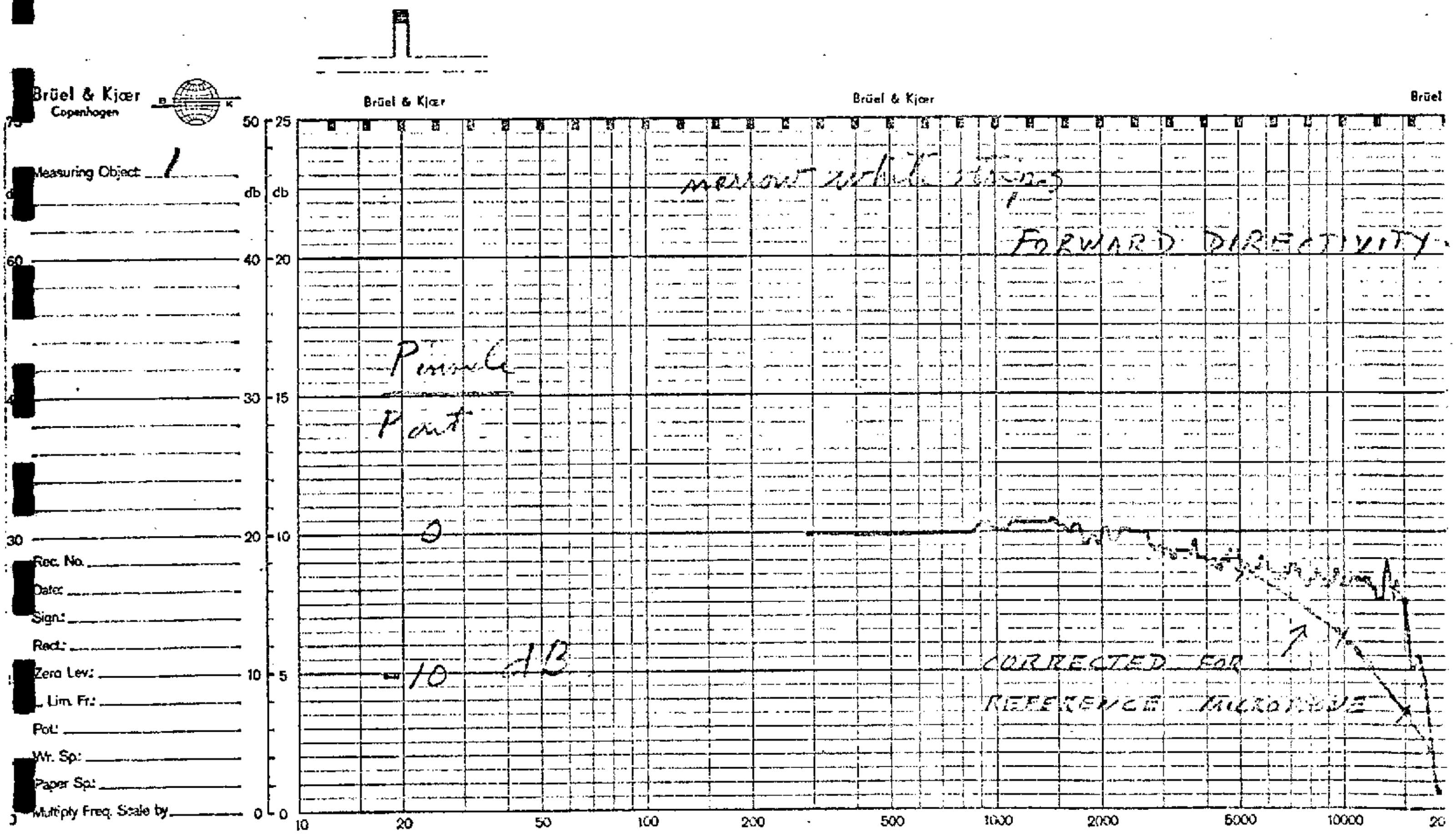

FIGURE A-2. FORWARD DIRECTIVITY OF NARROW STRIPE MICROPHONE

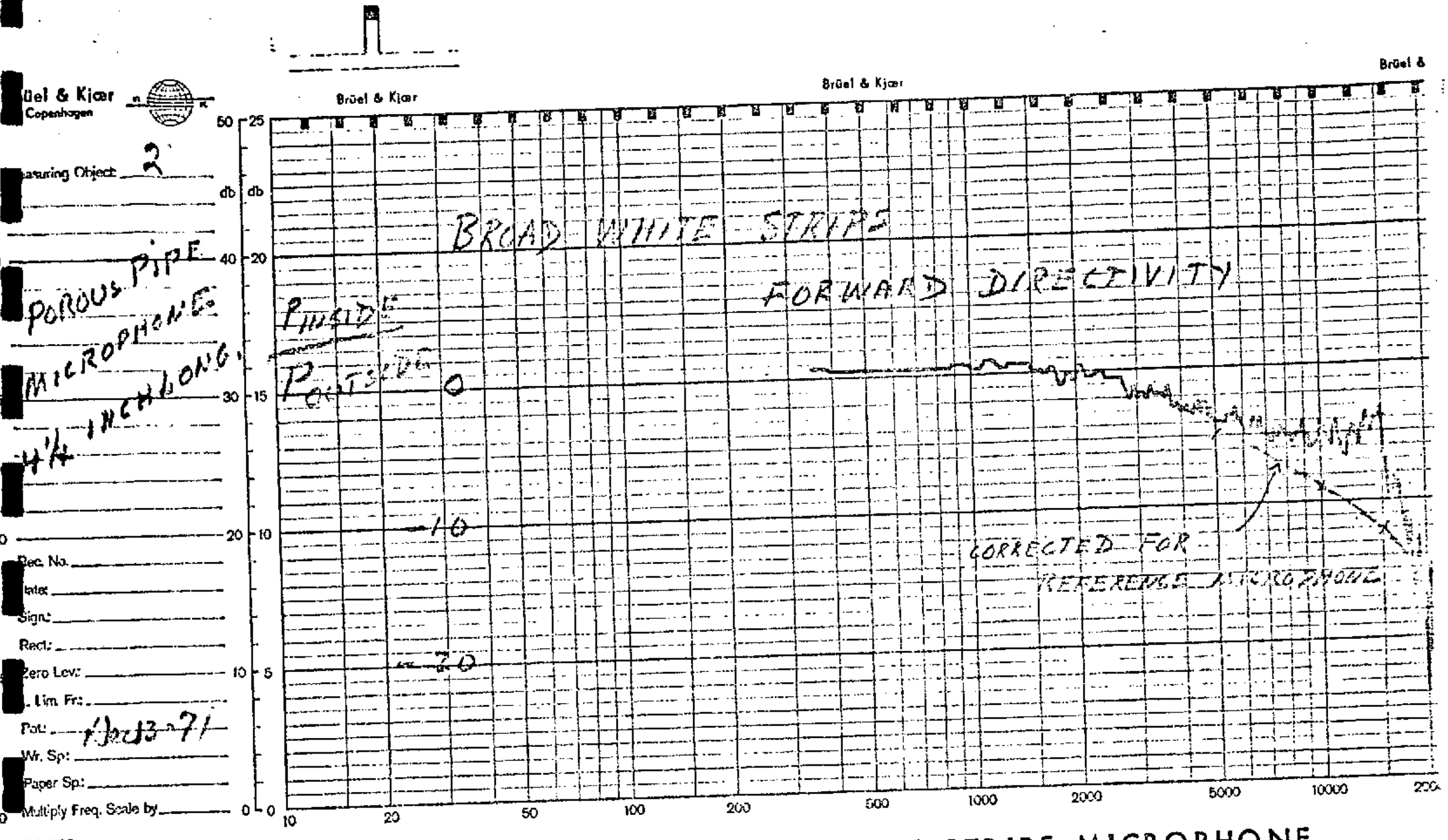

FIGURE A-3. FORWARD DIRECTIVITY OF WIDE STRIPE MICROPHONE

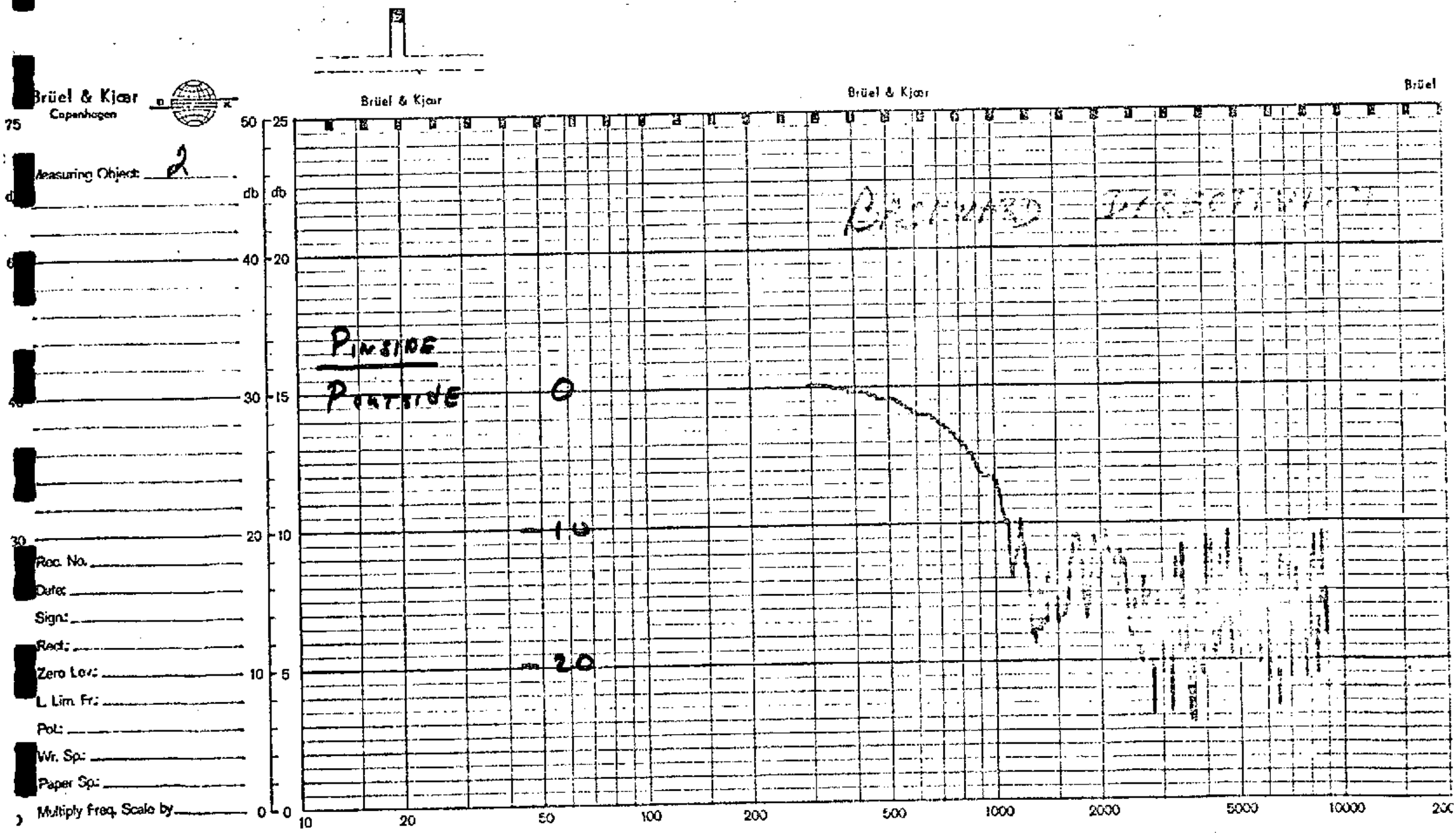

FIGURE A-4. BACKWARD DIRECTIVITY OF WIDE STRIPE MICROPHONE